Advances in Colloid and Interface Science 166 (2011) 87–118

Contents lists available at ScienceDirect

Advances in Colloid and Interface Science

journal homepage: www.elsevier.com/locate/cis

Reactive wetting, evolution of interfacial and bulk IMCs and their effect on mechanical properties of eutectic Sn–Cu solder alloy

Satyanarayan, K.N. Prabhu *

Department of Metallurgical and Materials Engineering, National Institute of Technology Karnataka, Surathkal, Mangalore 575 025, India

ARTICLE INFO

Available online 17 May 2011

Keywords:
Reactive wetting
Sn–0.7Cu lead-free solder
Contact angle
IMC

ABSTRACT

Lead free solders are increasingly being used in electronic applications. Eutectic Sn–Cu solder alloy is one of the most favored lead free alloys used for soldering in electronic applications. It is inexpensive and principally used in wave soldering. Wetting of liquid solder on a substrate is a case of reactive wetting and is accompanied by the formation of intermetallic compounds (IMCs) at the interface. Wettability of Sn–0.7Cu solder on metallic substrates is significantly affected by the temperature and the type of flux. The wettability and microstructural evolution of IMCs at the Sn–0.7Cu solder/substrate interfaces are reviewed in the present paper. The reliability of solder joints in electronic packaging is controlled by the type and morphology of interfacial IMCs formed between Sn–0.7Cu solder and substrates. The formation and growth mechanisms of interfacial IMCs are highlighted. Mechanical behavior of bulk solder alloy and solder joint interfaces are analyzed. The characteristics of the IMCs which have marked effect on the mechanical properties and fracture behavior as well as reliability of solder joints of the alloy are discussed. An attempt has also been made to discuss the effect of cooling rate and strain rate on shear strength, tensile properties and creep resistance of the solder alloy. It is recommended that future work should focus on evolving a standard procedure involving sequential assessment of wetting behavior, evolution of IMCs and mechanical properties.

Contents

1. Introduction

Eutectic or near eutectic Sn–Pb solder alloys are the most common solder materials used in the electronics industry because of their low melting point, better wettability, good mechanical, fatigue and creep properties [1]. The lead present in the solder material is highly toxic and considered to be hazardous to the environment [2]. Under the European Parliament and the Council of European Union, three directives have been initiated by the European Commission for restriction of use of Pb in electronic applications. These are WEEE (Waste Electrical and Electronic Equipment), RoHS (Restriction of use of Hazardous Substances) and ELV (End of Life Vehicle) directives. The

* Corresponding author. Fax: +91 8242474033.
E-mail address: prabhukn_2002@yahoo.co.in (K.N. Prabhu).

0001-8686/$ – see front matter © 2011 Elsevier B.V. All rights reserved.
doi:10.1016/j.cis.2011.05.005

U.S. Environmental Protection Agency (EPA) has banned the use of lead in paints since 1978. Japan passed 'Home Electronics Recycle Law' in 1998 [2]. These initiatives have lead to the development of new lead free solders like Sn–Cu, Sn–Ag, Sn–Zn–Bi, Sn–Ag–Bi, Sn–Bi, Sn–Ag–Cu, Sn–Ag–Zn, Sn–Zn, and Sn–In for electronic applications in which Sn is a major element [3–10]. Sn–Zn, Sn–Sb and Sn–Bi are cheap, but the presence of Zn in solder alloys leads to oxidation and corrosion, Sb is a very toxic element whereas eutectic Sn–Bi solders have reflow processing temperatures in the range of 180–200 °C which is lower than that of conventional Sn–Pb solders. Indium based systems have low liquidus temperatures. For example Sn–49.1In alloy has $T_{eu} = 117$ °C. The problem with indium and silver based solder alloy is volatility in pricing. Further Sn–Ag and Sn–Ag–Cu solders are expensive and the presence of excessive IMCs and voids at the interface are their major drawbacks.

The eutectic Sn–0.7Cu has been considered to be equally attractive as eutectic Sn–Pb in performance. Sn–0.7Cu solder alloy is used as alternative to lead based solder alloy due to its excellent physical and mechanical characteristics. It is lower in cost compared to other lead free solders and this has made it attractive for soldering in electronic applications [2,11–14]. Eutectic Sn–Cu solder alloy is principally used in wave soldering in electronic packaging field since 1998 [15]. Nortel Network is one of the famous lead free pioneers in Europe, which initiated a lead free program in 1991 and selected eutectic Sn–0.7Cu solder as the emerging lead free solder and built around 500 lead free telephones in 1998 [16]. Nortel further certified that Sn–0.7Cu solder has a soldering quality equal to Sn–37Pb and recommended it for wave and reflow soldering [16]. According to the National Electronics Manufacturing Initiative (NEMI) the leading lead free solder alloys to replace eutectic Sn–Pb are Sn–0.7Cu (first priority) and Sn–3.5Ag (second priority) for wave soldering applications. The Sn–0.7Cu alloy is suitable for high temperature applications like automotive industry [17]. It has shown a significant improvement in creep/fatigue data over Sn–Pb alloys [18]. It is also used in surface mount technology (SMT), plated through hole, ball grid arrays, flip chip technology [19]. The basic thermal properties of the solder alloy is given in Table 1 [20].

The Sn–Cu binary alloy has a eutectic composition of Sn–0.7Cu (wt.%) and a eutectic temperature of 227 °C [10]. The solidification phase transformation of solder is

$$\text{Liquid} \rightarrow \text{Sn} + \text{Intermediate phase}$$

$$\text{Eutectic reaction at 227 °C : Liquid} \rightarrow \beta\,\text{Sn} + \text{Cu}_6\text{Sn}_5.$$

The solidification reaction consists of Cu precipitated in the form of hollow rods of the intermetallic Cu_6Sn_5 [21]. Another good example for the formation of hollow rods of Cu_6Sn_5 within the solder alloy is the reaction between molten Sn–40Pb solder with Cu [22]. The solid solubility of copper in tin at eutectic temperature is only 0.006 wt.% or 0.01 wt.% and the intermediate phase corresponds to 44.8 to 46% Sn [2]. The solder is composed of large, Sn rich grains with a fine dispersion of Cu_6Sn_5 intermetallics. According to the phase diagram (Fig. 1 [23]), the stable intermetallic phases below 300 °C are ε and η phases. The ε phase has a composition close to Cu_3Sn and corresponding η has the composition of Cu_6Sn_5 [24]. Fig. 2a shows the microstructure of Sn–0.7Cu alloy. The primary tin dendrites dominate the microstructure of the alloy [25]. These tin dendrites disappear when nickel is present at the appropriate level (Fig. 2b). The effect of the nickel addition is to suppress the growth of pro-eutectic tin dendrites and promote solidification as a true eutectic [25,26].

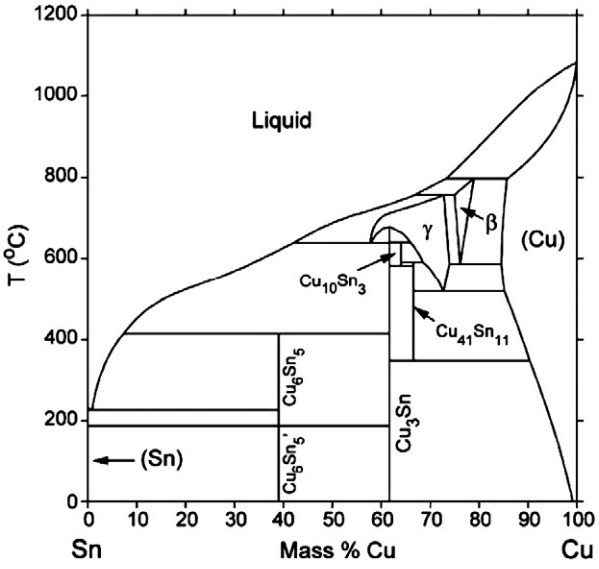

Fig. 1. Phase diagram of Sn–Cu system. [23].

Table 2 ranks the order of increasing environmental and occupational impacts with available toxicity of various Pb free solders [27]. Sn–0.7Cu is found to be less toxic in order as compared to Sn–5Bi–5Ag, Sn–2Ag, Sn–3.5Ag, Sn–3.2Ag–0.5Cu and Sn–5Sb solder alloys [27].

Cost is also one of the most important factors to be considered, while selecting a lead free alloy for electronic applications. Lead (Pb) is the least expensive element in soldering. Replacing Pb with other elements (Ag, Bi, In etc.,) in a solder alloy will increase the price. The eutectic Sn–0.7Cu is the cheapest among all other lead free solders and costs only 30% higher than the eutectic Sn–Pb solder. Density should be considered when comparing the cost of lead free alloys with that of Sn–Pb. Density and cost difference for various lead free solder alloys and Pb based solder are given in Table 3 [28]. Priorities given for various lead free solders in electronic application are given in Table 4 [29]. It confirms that Sn–0.7Cu is one of the emerging lead free solder that can be satisfactorily used for electronic and high temperature applications.

This paper reviews the recent developments related to wetting characteristics of solder alloy, importance of the formation and growth of intermetallic compounds between Sn–0.7Cu solder alloy and substrates and the assessment of the effect of IMCs on mechanical properties and solder joint reliability. The solder material selected is much cheaper compared to the Ag bearing Pb free solders. With the cost of silver increasing by more than 70% in the last year it is important that the research should focus on methods for improving the wettability and solderability of Sn–0.7Cu alloy.

Table 1
Basic thermal properties of eutectic solder alloy. [20].

Property	Sn–0.7Cu
Eutectic temperature (°C)	227
Latent heat of fusion (kJ/kg)	44.37
Thermal conductivity (W/m K)	53
Specific heat (J/kg-K)	223
Density (kg/m^3)	7300

2. Wettability of solder alloy on substrates

Wettting is a property of liquid solder or fluid to spread over a solid substrate, when brought in contact. Wettability can also be defined as the tendency for a liquid to spread on a solid substrate [30,31]. It describes the extent of intimate contact between a liquid and a solid.

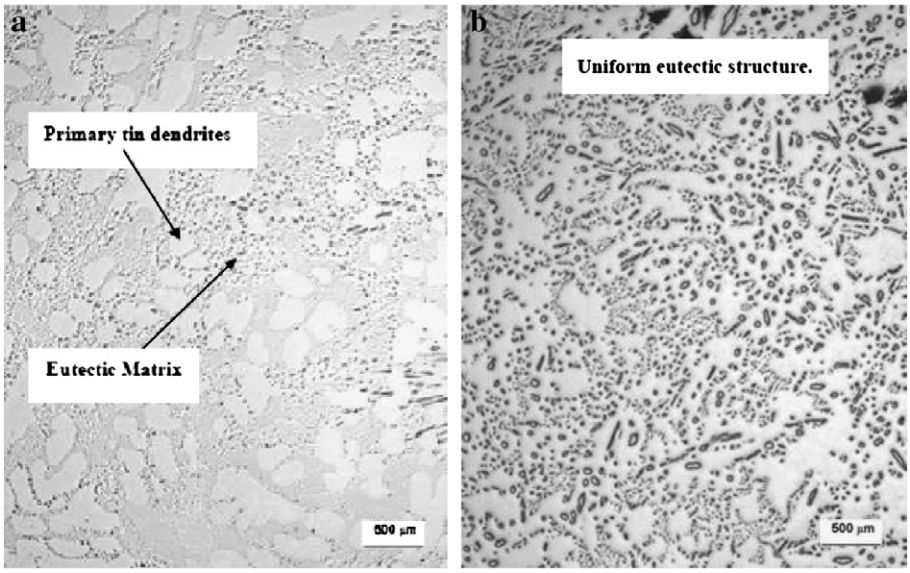

Fig. 2. (a) Micrograph of Sn–0.7Cu alloy, (b) effect of Ni addition on Sn–0.7Cu. [25].

Wetting is generally characterized by the degree and rate of wetting. The degree of wetting is generally indicated by the contact angle formed at the interface between solid and liquid. It is dependent on the surface and interfacial energies involved at the solid/liquid interface. The rate of wetting indicates how fast the liquid wets the surface and spreads over the same. It is guided by a number of factors such as the thermal conditions of the system, viscosity of the liquid and chemical reactions occurring at the interface, etc. [32]. Wetting force and contact angle are the two indices of wettability. The forces that determine the amount of wetting are known as wetting forces. A meniscograph method (wetting balance method) is one of the most commonly used wettability evaluation methods. In this method, a force on a substrate, while the substrate is immersed in a molten solder bath and is wetted by the solder, is measured as shown in Fig. 3 [33]. Indices of wettability, such as wetting time and wetting force, can be evaluated by the analysis of force–time curves (Fig. 4 [34]). The wetting force is given by the relation

$$F = P\,\gamma_{lf}\cos\theta - B. \quad (1)$$

F is the wetting force, θ is the contact angle, P is the perimeter of the solid substrate and γ_{lf} is the interfacial free energy of the solder–flux interface and B is the buoyancy force. Here P and B are constants. F and θ can be measured by using meniscograph tester (wettability tester) and γ_{lf} can be obtained from Eq. (1).

When a droplet of liquid sits on a solid surface, it will spread to some extent on the surface and then comes to rest making an angle with it as shown in Fig. 5. Contact angle is defined as, the angle between the tangent drawn at the triple point between the three phases (solid, liquid and vapor) and the substrate surface. Young's equation ($\gamma_{sv} = \gamma_{sl} + \gamma_{lv}\cos\theta_e$) provides a useful relation for the contact angle formed at the interface in terms of surface and interfacial tensions. Under equilibrium conditions this angle is decided by the surface and interfacial energies [1,32,34]. γ_{lv} is the surface tension between liquid and vapor phase. θ is the dynamic contact angle between the liquid and substrate and θ_e is the equilibrium contact angle attained after completion of spreading. θ_e can be measured using dynamic contact angle analyzer. Equilibrium contact angle θ_e measures the extent of wetting. For soldering application contact angles (θ_e) of up to 55° are found to be acceptable [1,35]. However if θ_e is less than 30° wetting is considered to be very good.

Rizvi et al. [36] studied the wetting behavior of Sn–0.7Cu solder on Cu and Ni based metals using wetting balance test method. The fluxes employed were NC (no clean) flux, WS (water soluble) flux and R flux at varying temperatures. They concluded that NC flux is suitable for Cu substrate and WS for Ni substrate at 255 °C, 275 °C and 295 °C. R flux is the worst for both substrates. Higher solder flux interfacial tension (445 mN/m) and poor cleaning capability of R flux are responsible for its worst performance. NC flux showed lowest value of solder flux

Table 2
Ranking of lead free solders in terms of toxicity. [27].

Sn–57Bi	Least impacts
Sn–20In	↓
Sn–0.7Cu	
Sn–5Bi–5Ag	
Sn–2Ag	
Sn–3.5Ag	
Sn–3.2Ag–0.5Cu	
Sn–5Sb	Greater impacts

Table 3
Comparison of costs of lead free solders. [28].

Alloy	Melting range (°C)	Density at 25 °C (lbs/in^3)	Metal cost per Δ Sn–37Pb
Sn–37Pb	183	0.318	0%
Sn–58Bi	139	0.316	+45%
Sn–20In–2.8Ag	179–189	0.267	+970%
Sn–9Zn	199	0.263	+13%
Sn–3.4Ag–4.8Bi	208–215	0.272	+125%
Sn–7.5Bi–2Ag–0.5Cu	186–212	0.273	+85%
Sn–2.5Ag–0.8Cu–0.5Sb	213–219	0.267	+95%
Sn–3.5Ag–1.5In	218	0.268	+190%
Sn–3.5Ag–3Bi	216–220	0.269	+110%
Sn–3.5Ag	221	0.368	+125%
Sn–0.7Cu	227	0.264	+23%
Sn–5Sb	232–240	0.263	+17%

Table 4
Industrial modeling list of priorities of materials properties.
[29].

	Sn–3.9Ag–0.6Cu	Sn–0.7Cu	Sn–3.5Ag	Sn–37Pb
CTE (liq. and solid state)	1	1	1	1
Vol. change on freezing (liq. and solid state)	1	1	1	1
Specific heat	3	3	3	3
Latent heat	3	3	3	3
Thermal diffusivity	3	3	3	3
Thermal conductivity	3	3	3	3
Electrical conductivity	3	3	3	3
Electrical resistivity	3	3	3	3
Surface tension at temp of solder	2	2	2	2
Wetting time at O force as f (temp) solder	2	2	2	2
Wetting time at 2/3 force as f (temp) solder	2	2	2	2
Max. wetting force as f (temp) solder	2	2	2	2
UTS at 25 °C	1	1	1	1
Shear strength (strain rates from 10^{-1} to 10^{-6} s^{-1})	1	1	1	1
Ring in plug (strain rates from 10^{-1} to 10^{-6} s^{-1})	3	3	3	3
E (Young's modulus) at 25 °C	1	1	1	1
E at 50 °C	1	1	1	1
E at 100 °C	1	1	1	1
E at 125 °C	1	1	1	1
Total elongation (strain rates from 10^{-1} to 10^{-6} s^{-1})	1	1	1	1
Uniform elongation at R^0 (strain rates from 10^{-1} to 10^{-6} s^{-1})	1	1	1	1
Yield strength at R^0 (strain rates from 10^{-1} to 10^{-6} s^{-1})	1	1	1	1
Work hardening coefficient (strain rates from 10^{-1} to 10^{-6} s^{-1})	1	1	1	1
Creep resistance (strain rates from 10^{-1} to 10^{-6} s^{-1})	1	1	1	1
Min. creep strain rate at stress of 20 Mpa at R^0	1	1	1	1
Min. creep strain rate at stress of 20 Mpa at 125 °C	1	1	1	1
Hardness	3	3	3	3
Thermomechanical Fatigue resistance (strain rates from 10^{-1} to 10^{-6} s^{-1})	1	1	1	1
Isothermal fatigue data (strain rates from 10^{-1} to 10^{-6} s^{-1})	1	1	1	1
Thermal fatigue hysteresis behavior (strain rates from 10^{-1} to 10^{-6} s^{-1})	1	1	1	1
Constitutive behavior (strain rates from 10^{-1} to 10^{-6} s^{-1})	1	1	1	1
Stress rupture (strain rates from 10^{-1} to 10^{-6} s^{-1})	3	3	3	3
Dynamic acoustic measurements	3	3	3	3
Fracture toughness at R^0 (strain rates from 10^{-1} to 10^{-6} s^{-1})	3	3	3	3

1 = high priority, 2 = medium priority, 3 = low priority.

interfacial tension (370 mN/m) and for WS flux the interfacial tension was found to be 415 mN/m. Increase in solder bath temperature lowers the value of contact angle because of the thermally induced changes to the flux molecular structure which contributes to lower value of solder flux interfacial tension. According to Hwang [37], wetting time (W_t) of Sn–0.7Cu solder decreases with the increase in temperature from 235 °C to 265 °C due to change in metallurgical reactions, surface tension and fluidity. At 245 °C wetting time (W_t) is close to 1 s and its wettability increases as the temperature increases to 255 °C. At 265 °C wetting time (W_t) is less than 1 s. As per ANSI/J-STD-003, the values of W_t are less than 1 s and 2 s for wave soldering and reflow soldering respectively. Sn–0.7Cu solder exhibited good solderability above 245 °C.

The contact angles of Cu by a molten Sn–0.7Cu alloy were reported by Mario et al.[38]. Sessile drop method was adopted to measure the

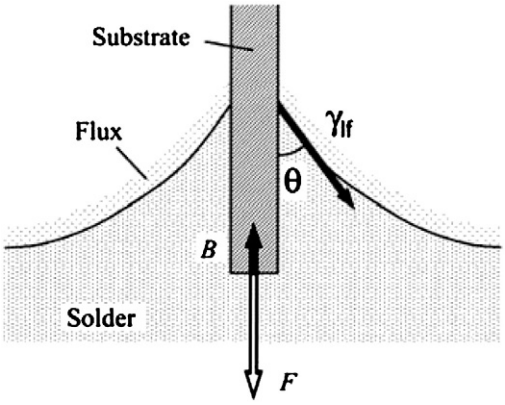

Fig. 3. Schematic diagram of wetting balance technique. F denotes the wetting force. γ_{lf} represents the interfacial free energy of the solder–flux interface.
[33].

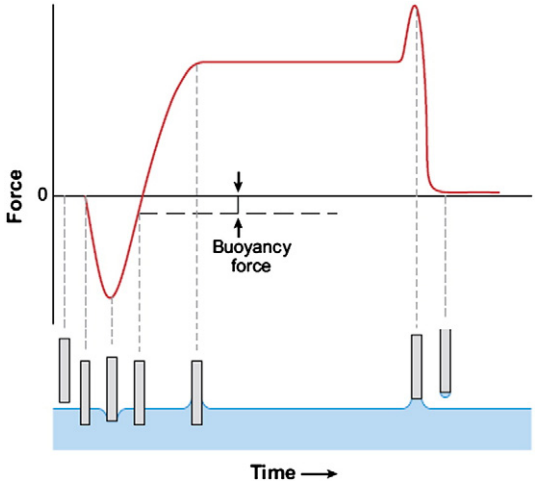

Fig. 4. Typical wetting curve in wetting balance technique.
[34].

contact angle. Temperature and flux (RMA and RA) were taken as variables. For the solder alloy, lower contact angles (19 to 30°) were obtained using RMA flux and RA flux compared to the test with no fluxes under vacuum (θ = 30°) and the contact angle decreased with increase in temperature. According to authors, the higher contact angles observed for solder might be due to the increase of the solder–vapor interfacial tension caused by the absence of lead. The Cu_3Sn IMC was not observed during wetting of solder using RMA flux and the same IMC occurred as thin layer when RA flux was used. This could be due to the difference in heat transfer coefficients of the fluxes. The heat transfer characteristics of the RA flux may not allow the

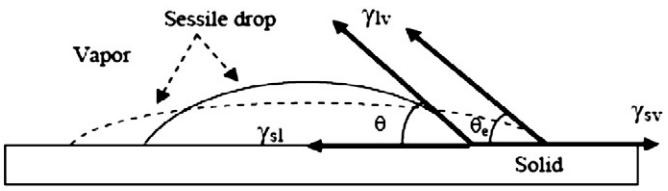

Fig. 5. Spreading of sessile drop on solid surface.
[23].

formation and growth of Cu_3Sn, because it requires higher temperatures to form. Experiments carried out with similar test conditions with R flux [39], yielded contact angles that were higher than the RMA and RA flux. This implies that R flux is not suitable for Sn–0.7Cu solder alloy on copper substrate.

An excellent work on reactive wetting of Sn–0.7Cu alloy on Cu and (Cu_6Sn_5/Cu_3Sn)/Cu substrates was reported by Wang et al. [40]. In this work, wetting balance test and hot stage test were carried out. For the solder alloy, the equilibrium contact angle (obtained from wetting balance test) on the IMC surface was smaller than the virgin copper substrate. The formation of Cu_6Sn_5 IMC at the interface of solder and IMC substrate is found to be greater than that of virgin Cu. A set of movie clips were captured during spreading of Sn–0.7Cu solder on virgin Cu substrates as shown in Fig. 6 (hot stage test). Eutectic Sn–Cu solder on IMC surface featured an average value of final wetting radii only slightly larger than that on a Cu based metal. The triple line velocity (the rate of spreading) was also greater than that for spreading on bare copper.

Viscosity is a very important physical property to be considered during wetting. In the process of electronic packaging, viscosity of solder affects the gap filling and solderability. The viscosity of the eutectic Sn–Cu solder alloy decreased with increasing temperature [41], whereas the surface tension of the solder decreased first with an increase in temperature up to a certain value after which it again started to increase slightly because liquid structure of the melts changed at these temperature zones. It is reported that if only wetting properties are considered, the suitable temperature to perform soldering of eutectic Sn–0.7Cu alloy is 303 °C (603 K), because solder exhibits a smallest value of surface tension (around 369 mN/m).

Wetting kinetics of solder was also studied using hot stage microscopy under nitrogen atmosphere. The RMA flux was used on pure Cu substrate to carry out the experiment. Spreading of the solder alloy showed two stages with a sharp change in the spreading rate. Halo region also appeared around the bulk solder domain. The EDS analysis of this region indicated the presence of Cu and Sn elements. It is believed that the formation of halo region is related to an interfacial reaction and to the formation of intermetallic layer. At the triple-line location a thin Sn-rich liquid precursor domain was also observed. Therefore, a limited-size halo observed around the bulk Sn–0.7Cu solder domain (Fig. 7) indicated that, mostly Sn was available in the layer for the reaction. The small halo region cannot additionally assist the liquid to move forward due to the lack of network like capillary action [42]. There are at least four distinct stages of wetting and spreading of solders. During the initial stage the solder forms a spherical cap and there is subsequent rapid spreading with a decrease in the contact angle. As the growth rate of IMCs increase the contact angle temporarily stabilizes. The situation continues for a few seconds followed by a further reduction in contact angle. This is thought to be allied with a progressive change in the composition of the solder resulting in a sudden change in IMCs formed in the halo at the edge of the solder liquid. Therefore, halo is considered as a feature of solder spreading [43]. It is a good example of preferential solder wetting and flow and it is characterized by the presence of an outer thin solder region (halo) and an inner circle consisting of the main mass of the solder droplet. Halo feature can result from differential heating and melting of the solder alloy and preferential wetting by one or more alloy constituent. Formation of halo region is usually not considered as a defect, but a sign of good wetting [44].

Zhao et al. [45] investigated the effect of spreading kinetics of liquid Sn–0.7Cu solder over an intermetallic solid surface. The three IMC surfaces were considered: (i) An IMC (Cu_6Sn_5/Cu_3Sn) layer formed without aging on Cu, (ii) an IMC layer formed after the Sn-coated Cu substrate was subjected to an aging process at 127 °C for 10 days, and (iii) an IMC surface formed after the Sn-coated Cu substrate was subjected to an aging process at 150 °C for 10 days. The reason for aging at higher temperature was to achieve larger grain size of the IMC interface reaction products. A part of the molten solder spreads on the IMC 1 surface like a thin film and showed a halo around the bulk molten solder. Solder spreading over IMC 2 and IMC 3 surfaces exposed to aging at elevated temperatures (having large grain sizes) did not indicate significant progress of wetting compared to bare copper substrates.

Sattiraju et al. [46] have examined the compatibility of Sn–0.7Cu solder and printed wire board (PWB). For the experimental work, the

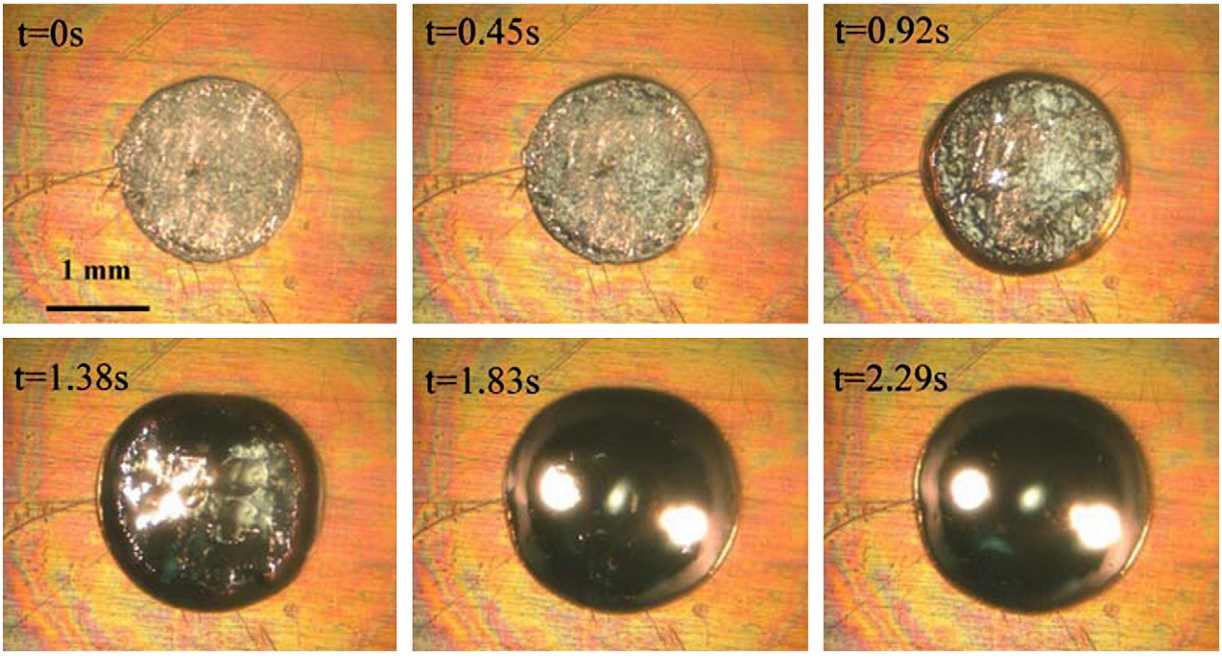

Fig. 6. Wetting progression of Sn–0.7Cu on Cu at 257 °C.
[40].

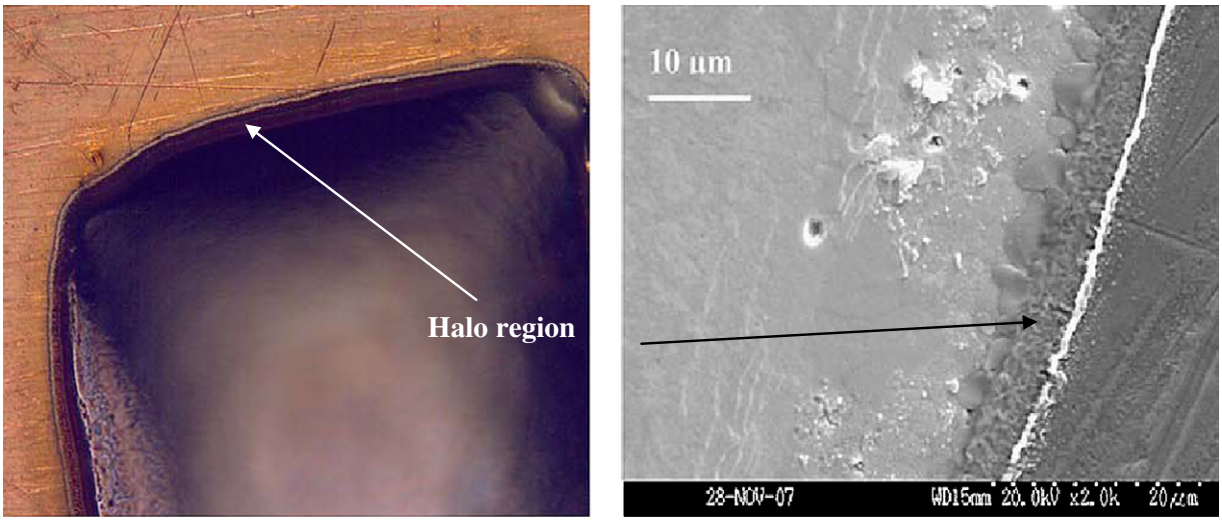

Fig. 7. Optical and SEM images of the halo region of resolidified Sn–0.7Cu solder on a Cu substrate. [42].

PWB test coupons were prepared using immersion in Sn, electroless Pd and Ni/Au, and immersion in Ag and OSP (organic solderable preservative). Water soluble flux (WS) and no-clean flux (NC) were used for wetting balance test. All surface finishes and both fluxes yielded satisfactory wetting results. The WS flux showed higher wetting force than no clean flux. For Sn finish eutectic Sn–Cu solder exhibited maximum wetting force and lowest for OSP and Pd finish. Wetting time was smaller for the OSP and Ag finishes and greater for Pd finish. The operating temperature for the above tests was 245 °C.

Electroplating is a commercially viable process as it offers simple manipulation and mass productivity. However, this plating technique easily suffers from poor uniformity. Even polishing efficiency of chemical mechanical polishing (CMP) is low. An improved effective polishing technique was developed by Hsu et al. [47], to control the uniformity of copper pillars. They used SPEEDFAM 15BTW polisher instead of a chemical mechanical polisher (CSP). Cu/Sn–0.7Cu layer was selected for the plating because of the wafer and chip uniformity of copper pillars which were bonded strongly without tilting.

Surface roughness is an important factor that has significant influence on the wetting of fluids/molten solders. Rough surface provides an additional interfacial area for spreading the liquid resulting in the increase of surface energy. But according to Nalagatla [23] the change in surface roughness of Cu substrate had no significant influence on the spreading behavior of eutectic Sn–Cu lead free solder. Wettability data of Sn–0.7Cu alloy on base metals and IMC substrates are given in Table 5.

3. Bulk IMCs in eutectic Sn–0.7Cu

The changes in microstructure and microhardness of as-reflowed Sn–0.7Cu solder balls were investigated during high temperature aging at 200 °C for 2, 4 and 8 h and at 150 °C for up to 1000 h in nitrogen atmosphere by Seo et al. [54]. The eutectic structure was totally broken and coarsened Cu_6Sn_5 particles were dispersed randomly in β-Sn phase after 2 h of aging (Fig. 8a and b). The initial size of Cu_6Sn_5 in Sn–0.7Cu was found to be around 1.8 µm in average diameter before aging. As the aging time increases the Cu_6Sn_5 particles become larger in size with an average diameter of around 7.8 µm (Fig. 8c and d). The Sn grain size was hardly changed until 100 h of aging at 150 °C. As the aging time increased up to 1000 h at 150 °C, the average size of Sn grains increased. After 100 h of aging the β-Sn was totally broken and IMC particles were significantly coarsened. The diffusion rate of solute atoms is slower and formation energy of Cu_6Sn_5 IMC is smaller at 150 °C than at 200 °C. It was observed that the growth rate of IMCs at 150 °C is about 100 times slower than at 200 °C. For the solder as the aging time increased at 200 °C, the hardness steadily decreased up to 8 h, because the fine eutectic structure was totally broken and Cu_6Sn_5 IMC particles coarsened during aging. For aging at 150 °C, the hardness of Sn–Cu solder decreased until 100 h, because the eutectic phase became discontinuous due to coarsening of IMCs particles without enough additional IMC precipitation. Increasing the aging period up to 1000 h the hardness remained more or less constant, because the coarsened IMC particles may not significantly affect the hardness changes.

Lauro et al. [55] have also investigated the microstructural changes during thermal and mechanical processing of Pb-free Sn–0.7Cu solder joint. Here the alloy pellet was subjected to compressive deformation of 10%, 20%, 30% and 50% in a universal testing machine. To study the effect of heat treatment, as-cast and/or deformed solder pellets were subjected to an annealing treatment at 150 °C for 48 h in nitrogen atmosphere. The typical microstructure of as-cast and annealed (150 °C, 48 h) solder alloy is shown in Fig. 9. Sn dendrites (white region) are dispersed uniformly in the matrix of the Sn–Cu eutectic structure (dark region) in the as-cast condition, while a recrystallized, large grain structure is observed in the annealed condition (Fig. 9a and b). The round Sn dendrite structure observed in the as-cast condition is extensively deformed according to the amount of plastic deformation. After annealing, the deformed microstructure had undergone a remarkable recrystallization process for each deformation level of 20%, 30%, and 50%. Higher the deformation, the finer is the recrystallized microstructure. The plastic deformation applied up to 50% in height reduction has produced a progressive refinement of the dendrite structure in Sn–0.7Cu alloy. The hardness of the alloy was lower than those of the smaller deformation (20%, 30%). The authors suggested that the amount of softening is independent of the plastic deformation. The solder alloy exhibited small amount of recrystallization after annealing at 150 °C for 48 h, with 20% or smaller amount of plastic deformation.

Thermal analysis and quenching experiments were performed on Sn–0.7Cu alloy [56]. Thermal analysis was carried out in a tapered stainless steel cup coated with a thin layer of boron nitride. In the experiment, solder Sn–0.7Cu solder samples were quenched at 120 s,

Table 5
Wettability data of Sn–0.7Cu on base metals and IMC substrates.

Substrate	Environmental state/flux used	Method	Experimental condition	Temperature (°C)	Wetting force (mN)	Contact angle (°)	Reference
Cu	NC	Wetting balance (WB)	10 mm × 2 mm × 0.2 mm ID: 3 and IS: 21 mm/s, 10 s	255	1.39		[36]
				275	1.54		
				295	1.65		
	WS	WB	10 mm × 2 mm × 0.2 mm ID: 3 and 21 mm, 10 s	255	1.33		[36]
				275	1.58		
				295	1.71		
	R flux	WB	10 mm × 2 mm × 0.2 mm ID: 3 and 21 mm, 10 s	255	1.13		[36]
				275	–		
				295	–		
Ni	NC	WB	10 mm × 2 mm × 0.2 mm ID: 3 and 21 mm, 10 s	255	0.19		[36]
				275	0.46		
				295	0.56		
	WS	WB	10 mm × 2 mm × 0.2 mm ID: 3 and 21 mm, 10 s	255	0.51		[36]
				275	0.79		
				295	No improvement		
	R flux	WB	10 mm × 2 mm × 0.2 mm ID: 3 and 21 mm, 10 s	255	Not wettable		[36]
				275			
				295			
Cu	RMA flux (Asahi's flux Fl2002)	WB	10 mm × 25 mm × 0.85 mm ID 5 mm, 10 s	235	4.3		[37]
				245	4.8		
				255	5.4		
				265	5.7		
Cu	RMA flux	Sessile drop (SD)	–	260		34.5	[41]
				360		26.3	
Cu	RMA flux (EC19S-8)/N_2	WB	5 mm × 30 mm × 0.3 mm	257	3.25	41	[40]
Cu_6Sn_5/Cu_3Sn/Cu	RMA flux (EC19S-8)/N_2	WB	5 mm × 30 mm × 0.3 mm ID:3 mm	257	3.37	36	[40]
Cu	Vacuum (no flux)	SD	2.5 cm × 2.5 cm HT: 2 min	238		35	[38]
Cu	RMA	SD	2.5 cm × 2.5 cm HT: 2 min	240		19	[38]
				260		19.5	
				280		17	
	RA	SD	2.5 cm × 2.5 cm HT: 2 min	240		30	[38]
				260		26	
				280		23	
Cu	R	SD	2.5 cm × 2.5 cm HT: 2 min	240		62	[39]
				260		54	
				280		52	
Cu	RA		40 mm × 40 mm × 2 mm, 60 s	260		49.96	[48]
						31.77	
Cu	WS (W-2348)	WB	0.5 mm × 1 mm × 15 mm ID: 4 mm	240	0.1733		[52]
Cu	WS (W-2348)	WB	0.5 mm × 1 mm × 15 mm ID: 4 mm	250	0.26		[52]
	RMA type	WB	0.5 mm × 1 mm × 15 mm ID: 4 mm	250	0.0967		[52]
	R type	WB	0.5 mm × 1 mm × 15 mm ID: 4 mm	250	0.0733		[52]
Ag	WS (W-2348)	WB	0.5 mm × 1 mm × 15 mm ID: 4 mm	240	0.1867		[52]
	RMA type	WB	0.5 mm × 1 mm × 15 mm ID: 4 mm	240	0.22		[52]
	R type	WB	0.5 mm × 1 mm × 15 mm ID: 4 mm	240	0.1867		[52]
Ag	WS (W-2348)	WB	0.5 mm × 1 mm × 15 mm ID: 4 mm	250	0.2933		[52]
	RMA type	WB	0.5 mm × 1 mm × 15 mm ID: 4 mm	250	0.24		[52]
	R type	WB	0.5 mm × 1 mm × 15 mm ID: 4 mm	250	0.2233		[52]
Ni	WS (W-2348)	WB	0.5 mm × 1 mm × 15 mm ID: 4 mm	240	0.1633		[52]
Ni	WS (W-2348)	WB	0.5 mm × 1 mm × 15 mm ID: 4 mm	250	0.2167		[52]
Cu	RMA/N_2 atm (Tamura, EC-19S-8)	WB	5 mm × 30 mm × 0.3 mm ID:3 mm, 10 s	260		42.5	[50,51]
Cu	NC	WB	10 mm × 2 mm ID:3 mm	255	1.39	56	[53]
				275	1.54	54	[53]
				295	1.65	50	[53]
Ni	WS	WB	10 mm × 2 mm ID:3 mm	255	0.51	72	[53]
				275	0.72	63	[53]
				295	0.76	62	[53]
PWB with immersion Sn finish	WS	WB	0.25 in. × 0.062 in., ID 5 mm, 10 s	245	8.8		[46]
	NC				6.8		
PWB with immersion Ag finish	WS	WB	0.25 in. × 0.062 in., ID 5 mm, 10 s	245	8.8		
	NC				7.2		
PWB with electroless Ni/immersion Au	WS	WB	0.25 in. × 0.062 in., ID 5 mm, 10 s	245	8.2		[46]
	NC				6.5		
PWB with electroless Pd	WS	WB	0.25 in. × 0.062 in., ID 5 mm, 10 s	245	6.5		
	NC				4.8		
PWB with OSP	WS	WB	0.25 in. × 0.062 in., ID 5 mm, 10 s	245	7.1		
	NC				4.4		
Cu	RA	SD	15 mm × 15 mm	250		41.1	[49]

NC: no clean, RMA: rosin mildly activated, RA: activated rosin.
WS: water soluble, WB: wetting balance technique, SD: sessile drop method, CA: contact angle.
ID: immersion depth, IS: Immersion speed, HT: heating time, PWB: printed wiring board.
OSP: organic solderable preservative.

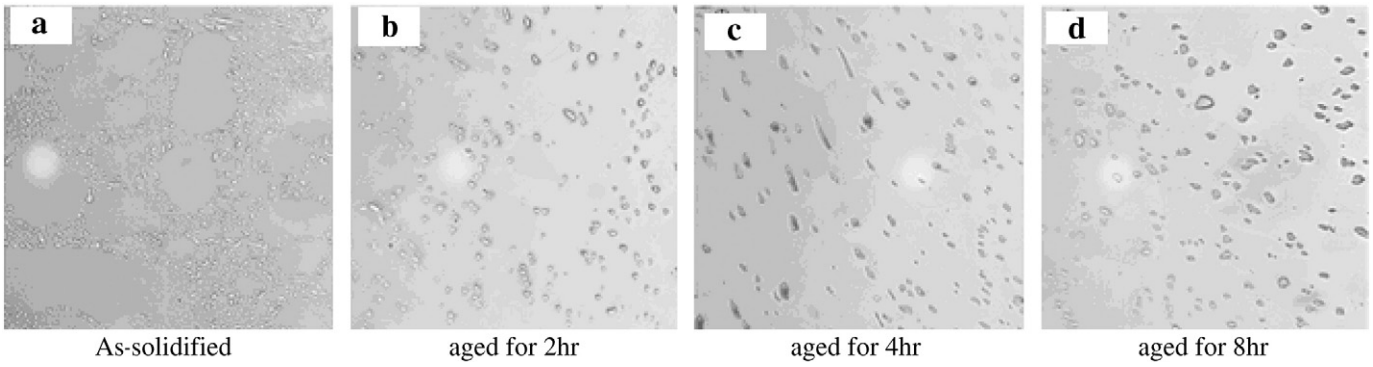

Fig. 8. Bright optical images of Sn–Cu as-reflowed and aged at 200 °C for 2, 4 and 8 h. [54].

220 s and 320 s from the point of maximum undercooling. Fig. 10a shows the optical micrograph of fully solidified Sn–0.7Cu and Fig. 10b shows Sn–0.7Cu solder microstructure quenched during different stages. In fully solidified Sn–0.7Cu alloy the morphology of Cu_6Sn_5 is relatively coarse and needle like. In the quenched samples a few large dendrites of Sn grow preferentially from the base of the sample. In Fig. 10b the darker area is liquid at the time of quenching and the whiter area is the combination of primary Sn and Sn–Cu_6Sn_5 eutectic which solidified before quenching. The solidification process here takes place under non equilibrium conditions. A common problem for such phenomena is to establish a consistent theory predicting the morphology of the interface as a function of its velocity field [57]. Nogita et al. examined the mechanism underlying the improvement in soldering properties of Sn–0.7Cu eutectic alloys modified with concentration of Ni ranging from 0 to 1000 ppm. The alloys were investigated by thermal analysis during solidification, as well as optical/SEM microanalysis of fully solidified samples and samples quenched during solidification. Nogita et al. concluded that Ni additions dramatically altered the nucleation patterns and solidification behavior of the Sn and Sn–Cu_6Sn_5 eutectic. The changes observed were related to the superior soldering characteristics of the Ni modified Sn–0.7Cu alloys. They also suggested that the solidification

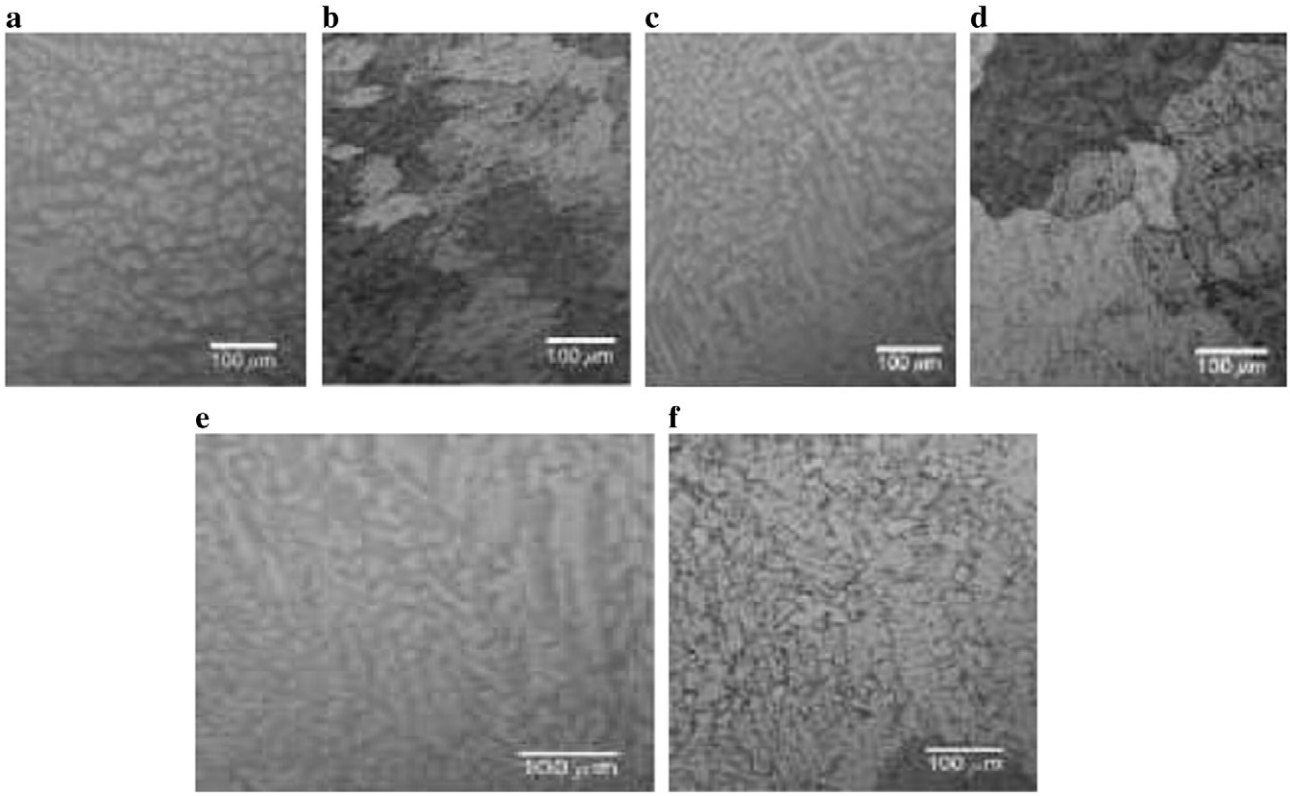

Fig. 9. Microstructure of Sn–0.7Cu solder alloy (a) in as-cast condition 0% deformed (b) after annealing at 150 °C, 48 h (0% deformed) (c) in as-cast condition 20% deformed (d) after annealing at 150 °C, 48 h (20% deformed) (e) in as-cast condition 30% deformed (f) after annealing at 150 °C, 48 h (30% deformed). [55].

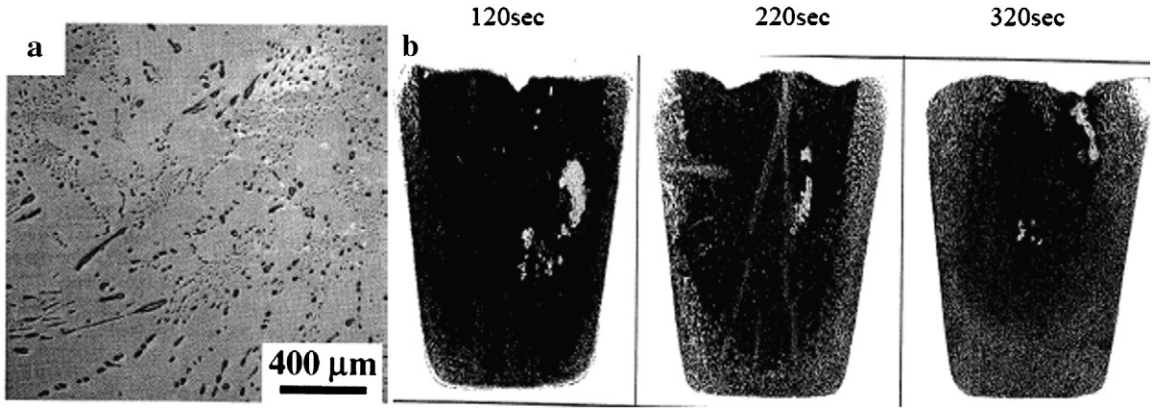

Fig. 10. (a) Optical micrograph of fully solidified Sn–0.7Cu. (b) Quenched microstructure during different stages of solidification. [56].

front advances from the edges of the samples towards the center in the bulk solder alloy. The solidification front is a semisolid or mushy zone with a fraction of liquid. The growth mode of mushy interface was called as the wall mechanism. Addition of 600 and 1000 ppm Ni to this alloy resulted in a change in the microscopic growth interface, with solid evolving from a large number of nucleation centers throughout the melt. The eutectic Sn–0.7Cu alloy exhibits hypoeutectic microstructure, consisting of a mixture of primary β-Sn dendrites and gray eutectic colonies when rapidly cooled (6×10^3 K min^{-1}) in a water cooled copper mold. Slowly cooled Sn–0.7Cu follows the corresponding equilibrium solidification path, i.e. liquid → β-Sn + intermediate phase [58].

Tin pest is one of the failure modes of electronic products. Tin undergoes an allotropic transformation of β-Sn (BCT) into α-Sn (diamond cubic) at temperatures below 13 °C. The transformation product is termed as "tin pest", and the change is accompanied by an increase in volume of 27%. Peng [59] examined the occurrence of tin pest in eutectic Sn–0.7Cu solder alloy. He used the cold rolled solder plate of size 1 mm thick. Tin pest of solder alloy was studied after a low temperature storage process at −196 °C for 50 h, −40 °C for 4 years, and −17 °C for 1.5 years (Fig. 11). It was reported that the eutectic Sn–Cu alloy did not show any indication of tin pest after going through the complete storage process.

However, Kariya et al. [60] observed tin pest on the surface of Sn–0.5Cu alloy after storage at −18 °C for 1.5 years. The affected area increased with the storage time. The conditions of the samples used in these two studies were completely different. Samples used by Kariya et al. were cast alloy ingots, but Peng used rolled alloy sheets. By rolling of solder ingot, the Sn grains were elongated, the Cu_6Sn_5 particles were broken into smaller particles, areas of grain boundaries increased, and dislocations and residual stresses were generated. These factors strengthened the alloy, making the allotropic change of β-Sn to α-Sn more difficult. Thus formation of tin pest was delayed.

Joo and Takemoto [61] observed that the formation of tin pest was promoted on rolling of Sn–0.8Cu alloy which contradicted the findings of Peng. However, the important point to be noted here is that Joo and Takemoto prepared the solder alloy in a graphite crucible. According to the Peng, during this time carbon might have been dissolved into the solder alloy and played a role in the promotion of tin pest formation. Peng clearly reported that further study is necessary to clarify this. Another possible reason for the difference between results represented by Peng and those made by Joo and Takemoto is that the rolled samples used by Peng were stored at room temperature for more than six months before the low temperature aging study. The deformation energy stored in the samples by rolling might have been partially consumed by stress relaxation and microstructural changes such as coarsening, as the room temperature itself is a high temperature for solder alloys.

4. Evolution of interfacial IMCs on various substrates

The formation of intermetallics between the molten solder and substrate is the case of reactive wetting. It is well known that the occurrence of the intermetallic compounds (IMCs) between solders and substrate metals is an indication of good metallurgical bonding [31,62]. A thin, continuous and uniform IMC layer is an essential requirement for good bonding [63,64]. However, due to their inherent brittle nature and the tendency to generate structural defects, too thick IMC layer at the solder/conductor metal interface may degrade the reliability of the solder joints [64]. For example, a small duration of peak temperature results in an in-complete wetting and cold joint formation. On the other hand, too high peak temperature or prolonged peak temperature duration may result in the formation of a brittle joint. Thus, a knowledge of the solder/substrate (conductor) metal interactions and phase evolution in solder interconnections is essential for the understanding of the reliability of solder joints from the metallurgical viewpoint and for the optimization of the soldering process. The

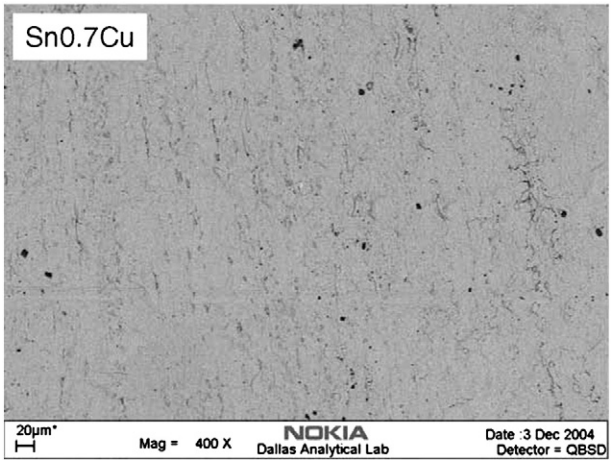

Fig. 11. SEM image of surface of the rolled Sn–0.7Cu solder plate subjected to low temperature storage process. [59].

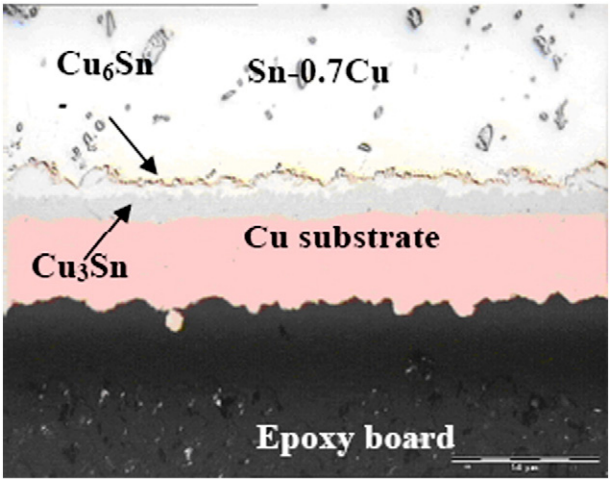

Fig. 12. Micrograph of the Sn–0.7Cu/Cu interface at 150 °C for 500 h. [65].

formation of interfacial IMCs on various metallic substrates is discussed in the following sections.

4.1. Copper

Copper is widely used in electronic applications because it has superior thermal and electrical conductivities. The evolution of microstructure in the interfacial region after thermal aging at 150 °C for 500 h was studied by Madeni [65] on Cu plated epoxy board. It was observed that a layer of Cu_3Sn forms at the interface and Cu_6Sn_5 layer on top of Cu_3Sn. The Cu_3Sn intermetallic layer growth front was less irregular than of the Cu_6Sn_5 (Fig. 12). Thickness and activation energies for the total IMC were found to be 14.1 μm and 0.68 eV/atom respectively.

Nogita [66] studied the cracking in reaction layers between Sn–Cu alloy and copper substrate using two soldering techniques: (i) BGA (ball-grid-array) soldered joints in which solder balls of 500 μm diameter on organic solderability protection (OSP) Cu boards with a common reflow process were used (Fig. 13a). The other soldering technique is by using (ii) dipped copper plate joints. In the second technique dipped Cu samples were prepared by dipping a Cu plate in the solder alloy. Cracks were observed within the Cu_6Sn_5 IMC layer for both the joining techniques. This was attributed to the method of sample preparation and the brittle IMCs implanted in a soft Sn matrix. Fig. 13b and c shows the cracked region in the IMC layer.

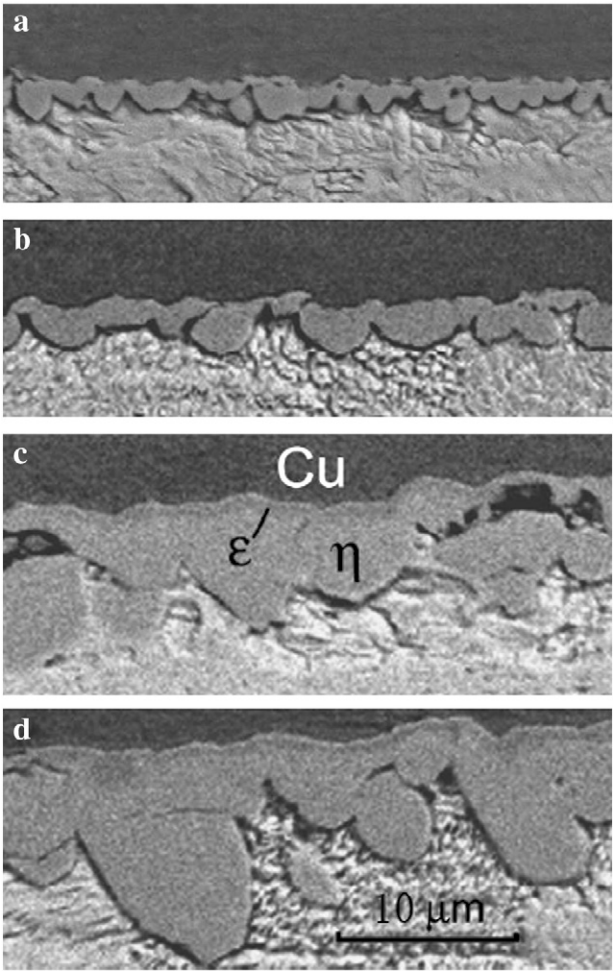

Fig. 14. BSE SEM images of the IMC layers formed between Cu substrate and Sn–0.7Cu solder held at 235 °C for (a) 10 s (b) 180 s (c) 1800 s and (d) 7200 s. [67].

The IMC growth kinetics for eutectic Sn–0.7Cu solder on Cu based metal is investigated by Dariavach et al. [67]. A thick scallop layer of η-Cu_6Sn_5 and a thin layer of ε-Cu_3Sn were observed at the interface. The total thickness of IMC and the grain size of the η phase increased with increasing soldering time for Sn–0.7Cu solder as shown in Fig. 14. The calculated apparent activation energy for the IMC growth of solder was found to be about 22.2 kJ/mol.

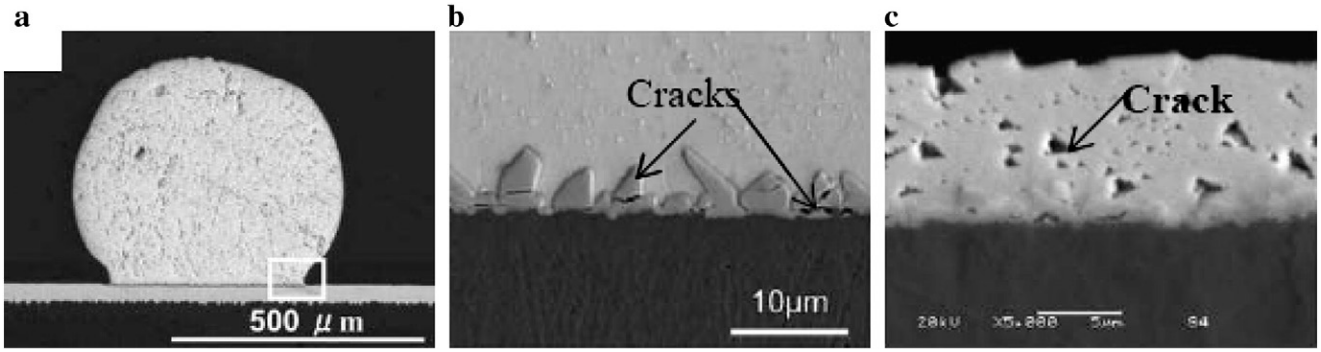

Fig. 13. (a) A typical cross-sectioned ball grid array on Cu substrate. (b) Cross-sectioned sample of BGA type showing cracks. (c) Cross-sectioned sample of dipped Cu substrate showing the cracks. [66].

As the interfacial reaction occurs between substrate and the molten solder, the liquid structure of solder significantly affects the reaction and the formation of interfacial compounds. Zhao et al. [68], studied the liquid structure of Sn–0.7Cu by using X-ray diffraction. Interfacial reaction between Sn–0.7Cu and Cu joints at 260 °C for 300 s were also studied. For Sn–Cu solder, Ashcroft–Langreth structure factor S(Q) showed a parabolic shape before the main peak and no pre-peak was detected. The reason is solubility of Cu in eutectic Sn–0.7Cu solder is lower than the solubility limit of Cu in pure Sn (1.61 wt.% at 250 °C). The liquid solder alloy did not exhibit the medium-range order (MRO). The liquid structure of solder alloy is found similar to that of pure Sn. The interfacial microstructure of solder joints reacted for 300 s exhibited Cu_6Sn_5 IMC layer at the interface.

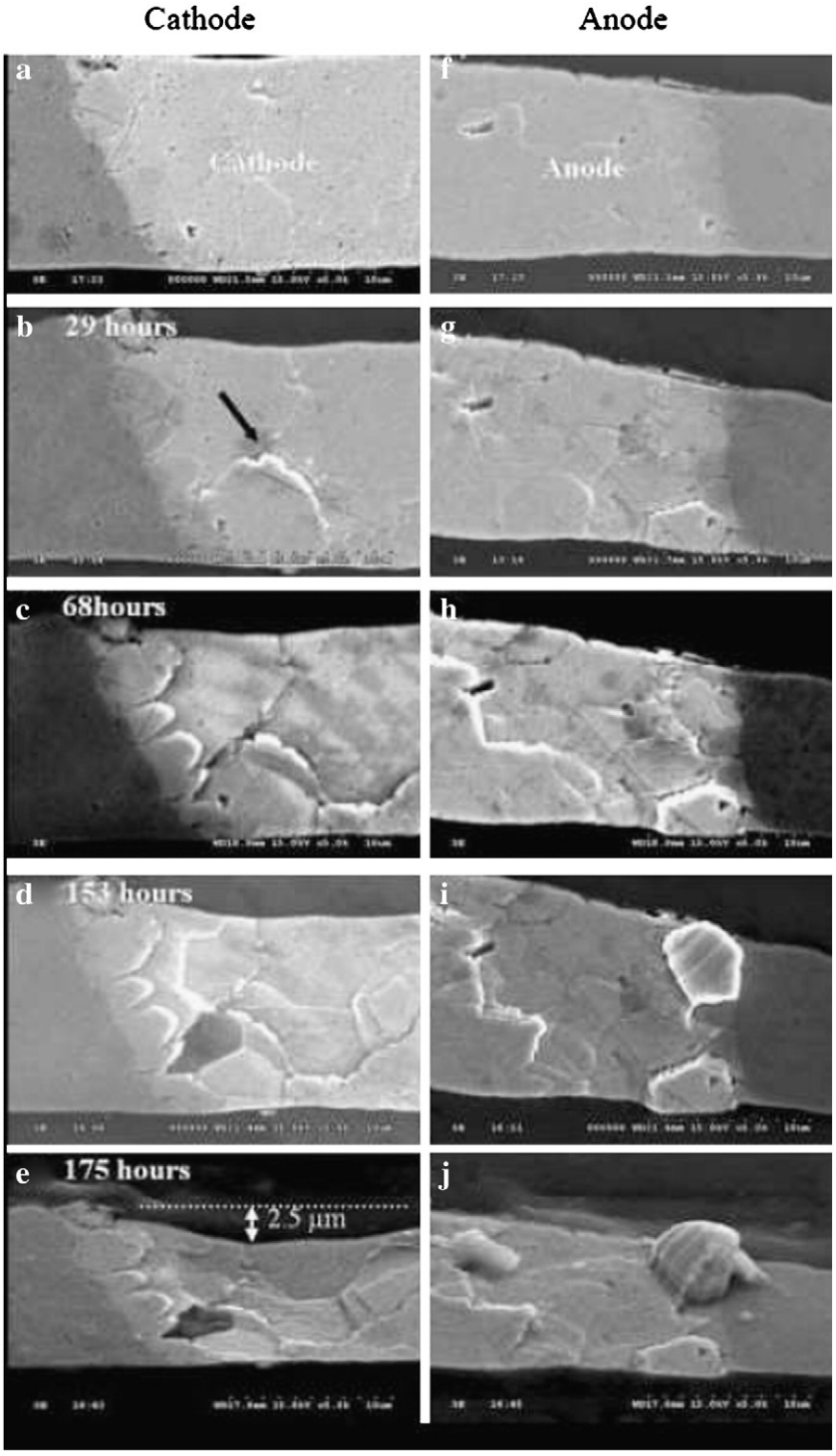

Fig. 15. Evolution of EM (electromigration) damage for the Sn–0.7Cu solder line at both the anode and cathode sides. [71].

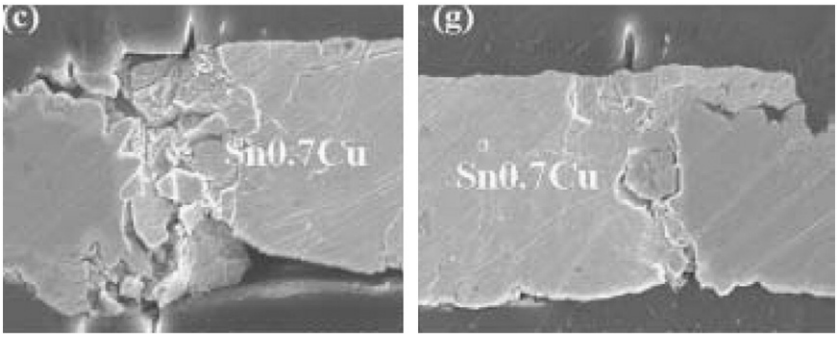

Fig. 16. SEM images of solder lines after 1-hr EM test at the elevated temperature of 100 °C showing fractures. [71].

A strong crystallographic orientation relationship between the Cu_6Sn_5 scallops type grains and the Cu substrate in the wetting reaction between molten Sn-based solders and Cu has been determined by Suha et al. [69]. They used Synchrotron Micro-X-ray diffraction for the study. To investigate reactions between Pb-free solders and Cu, they used pure Sn to represent various Pb-free solders (because compositions of most of Pb-free solders are nearly pure Sn). Angular distributions of crystallographic directions between Cu_6Sn_5 and Cu revealed a strong orientation relationship. The strong orientation relation suggested that Cu_6Sn_5 forms prior to Cu_3Sn in the wetting reactions. It was also reported by the same researcher [70] that Cu_6Sn_5 has a unique scallop-type morphology and Cu_3Sn has a layer-type morphology. The latter forms between the former and the copper substrate [70].

Six types of the orientation relationship between Cu_6Sn_5 and Cu were observed [69]. In all of them, the $[\bar{1}01]$ direction of Cu_6Sn_5 was always parallel to the [110] direction of Cu with a misfit of 0.24%. The six orientation relationships were classified into two groups because of the strong pseudohexagonal symmetry of Cu atoms in Cu_6Sn_5. Relationships involving planes (010), (343), and $(\bar{3}4\bar{3})$ belong to the first group. Relationships with planes (101), (141) and $(\bar{1}4\bar{1})$ belong to the second group. It was also found that the orientation distribution of Cu_6Sn_5 scallops is rather random in the early stage of reaction. As the reflow time increased, the Cu_6Sn_5 scallops gradually gain texture but the texture starts to decrease with further increase of the reflow time because of the growth of Cu_3Sn between the Cu_6Sn_5 and the Cu [69].

Electromigration is defined as the mass transport induced by the electrical field or charge carriers which often causes open failure and cracking in the microelectronic circuit or interconnects. The electromigration effects in metallic interconnect lines cannot be completely prevented but can only be improved by reducing the diffusivity of migrating atoms and modifying the microstructure of the materials [71]. Lu et al. [71] investigated the electromigration (EM) of Sn–0.7Cu on copper foils indicating that, the Sn–0.7Cu solder line has the most serious electromigration (EM) damage for the shortest length of 250 μm compared to longest solid lines (350 and 450 μm). The evolution of EM damage for the Sn–0.7Cu solder line at both the anode and cathode sides is shown in Fig. 15. Voiding was apparent at the cathode side, starting at the triple point of grain boundaries. At the anode interface, a small amount of Sn grains was pushed moderately out of the surface of the solder line after about 30 h of stressing. After 175 h of stressing, two large Sn grains were extruded out of the surface of the solder line. At the anode side, the hillock formation (4 μm in height) was observed and the depth of depletion at cathode was around 2.5 μm (Fig. 15). The hillock formation was observed at the anode sides after 175 h of current stressing. The hillock formation was attributed to the critical yielding stress for the grain-boundary sliding and dislocation motion. Lu et al. [71] carried out 1 h EM test at the elevated temperature of 100 °C for the solder line. They found that, fractures were observed at the cathode sides of the solder line (Fig. 16). The external stress induced by the CTE mismatch at 100 °C and EM tensile stress caused the fatal fracture at the cathode side. A novel failure mode of EM test was also observed by the researchers i.e., EM under an external tensile stress. For specimens stressed at the elevated temperature, the CTE mismatch between Cu–solder–Cu line and epoxy exerted a steady external tensile stress on the solder line. This external stress is superimposed on the stress profile induced by EM. As a result, the hillock formation was retarded at the anode side, and void formation was improved at the cathode.

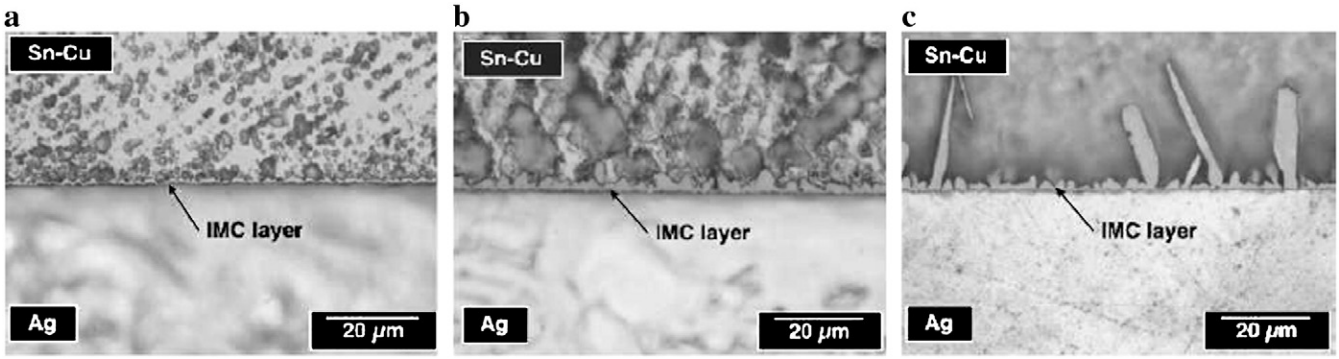

Fig. 17. Optical micrographs of Sn–0.7Cu/Ag tab interface produced by the liquid solder at (a) 260 °C/30 s, (b) 290 °C/30 s and (c) 320 °C/30 s. [72].

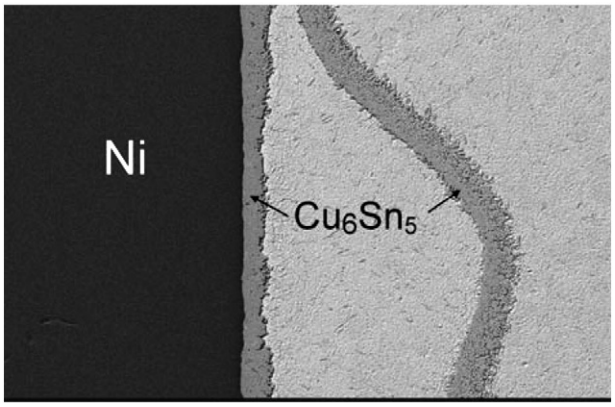

Fig. 18. The backscattered-electron image (BEI) micrograph of the eutectic Sn–Cu/Ni substrate reacted at 250 °C for 4 h.
[73].

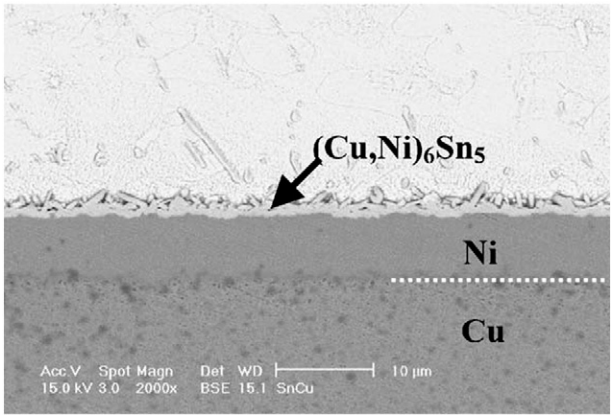

Fig. 19. SEM micrograph of the Sn–0.7Cu solder/Ni interface reflowed at 250 °C for 60 s.
[75].

4.2. Silver

Silver (Ag) and silver based alloys are widely used in electronic applications for the assembly of relay and other switching components. Vianco et al. [72] investigated the dissolution behavior and the IMC layer growth kinetics between Sn–0.7Cu and Ag substrate. Ag tabs were immersed into the molten Sn–0.7Cu solder bath at 240, 260, 290, 320 and 350 °C. The immersion times were 5, 15, 30, 60, 120 and 240 s. Eutectic Sn–0.7Cu/silver substrate exhibited blocky and needle shaped protrusions in the solder field as shown in Fig. 17. As the solder bath temperature and exposure time is increased, blocky and needle shaped protrusions increased monotonically. Continuous thin IMC layer devoid of protrusions, with some IMC particles having composition equivalent to Ag_3Sn was found within the solder field, for temperatures of 240 °C and 260 °C and exposure times of 5 to 60 s.

The authors represented the silver dissolution kinetics in the solder in terms of the equation

$$\Delta x = At^n \exp(-\Delta H / RT) \quad (2)$$

where A is a constant (m-$s^{1/n}$), t is time (s), n is the time exponent, ΔH is the apparent activation energy (kJ/mol), R is the universal gas constant (8.314 kJ/mol-K), and T is the temperature (K). The values of n and ΔH were 0.91 ± 0.05 and 37 ± 4 kJ/mol respectively for the eutectic Sn–Cu solder. The growth kinetics of IMC layer was also determined. The values of n and H for IMC layer growth kinetics were 0.22 ± 0.12 and 49 ± 9 kJ/mol respectively.

4.3. Nickel

The understanding of transformation of phase and the evolution of microstructure at the solder joint during soldering operation has become crucial in electronic applications, because reaction layer detachment is a typical apparent fact observed in the joint between Sn–Cu alloy and nickel substrate. Ni is frequently used as a diffusion barrier material of UBM in flip chip and BGA technology to prevent the rapid interfacial reaction between solders and Cu substrates.

Chen et al. [73] reviewed the phase transformation and microstructure evolution in Sn–0.7Cu/Ni solder joint. In addition to the reaction layer attached to the Ni based metal, a detached Cu_6Sn_5 phase layer with higher Ni solubility is observed for eutectic Sn–Cu/Ni couple at 250 °C for 4 h. The bonded layer shown in Fig. 18 has a dense structure and the separated layer has a loose structure, composed of tiny Cu_6Sn_5 particles. Longer exposure time resulted in a Ni_3Sn_4 phase adjacent to the Ni based metal. For eutectic Sn–Cu/Ni system, two kinds of detachments will exist. During the initial reaction, the Cu_6Sn_5 layer fractures and the loose layer separates from the attached Cu_6Sn_5 layer. At the final stage, the Cu_6Sn_5 layer separates from Ni_3Sn_4 phase.

Yoon et al. [74] investigated the interfacial reaction, shear strength and growth kinetics of IMCs formed between eutectic Sn–Cu solder/Au/Ni/Cu substrate i.e., Ni BGA joints, during isothermal aging at temperatures between 70 and 170 °C for up to 100 days. After reflow, the $(Cu,Ni)_6Sn_5$ IMC formed at the interface. Only $(Cu,Ni)_6Sn_5$ IMC

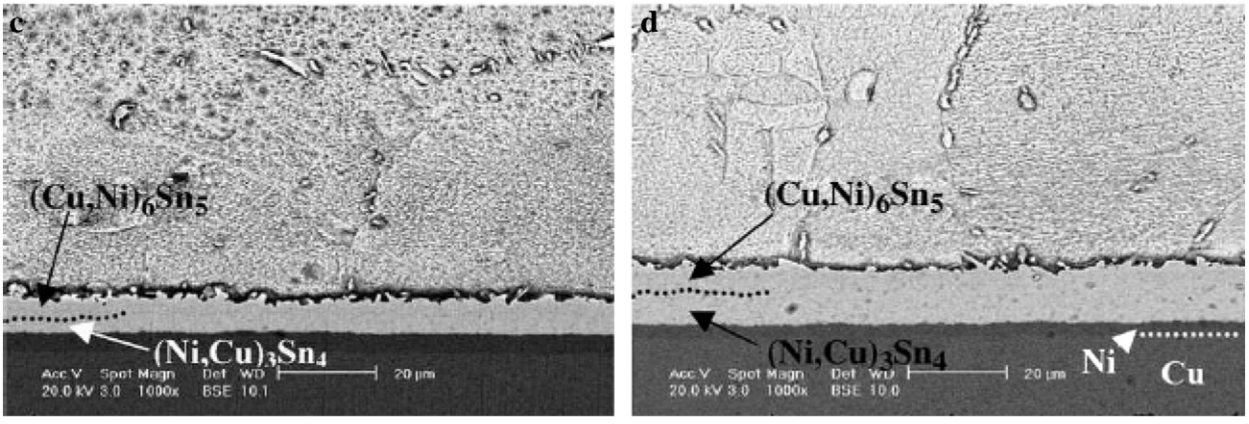

Fig. 20. SEM micrographs of the Sn–0.7Cu solder/Ni BGA joints aged at 185 °C for (c)15 days and (d) 50 days.
[75].

layer was observed at the interface of the samples aged at temperatures between 70 and 150 °C. After isothermal aging at 170 °C for 50 days, the Sn–Cu solder/Ni interface showed a duplex structure of $(Cu,Ni)_6Sn_5$ and $(Ni,Cu)_3Sn_4$. The shear strength decreased after aging for initial 1 day and then remained nearly unchanged with prolonged aging. Fracture occurred in the bulk solder.

Yoon and Jung [75] also investigated the influence of isothermal aging on the interfacial reaction and shear strength of Sn–0.7Cu/Ni BGA substrate during high temperature aging at 185 °C and 200 °C for a period of 60 days. During initial reflow (250 °C, 60 s), after entire Au layer dissolved into the molten solder, $(Cu,Ni)_6Sn_5$ was observed at the solder/Ni interface as shown in Fig. 19. After aging at 185 °C for 15 and 50 days $(Cu,Ni)_6Sn_5$ and $(Ni,Cu)_3Sn_4$ were observed (Fig. 20). The same IMCs were observed even for aging at 200 °C for 1 day. However the growth of the $(Ni,Cu)_3Sn_4$ IMC layer at this temperature was much faster than that in the earlier case. $(Ni,Cu)_3Sn_4$ IMC layer consumed the $(Cu,Ni)_6Sn_5$ IMC during its growth period at an aging temperature of 200 °C due to the restriction of supply of Cu atoms from the solder to interface (Fig. 21). The Ni layer of the base metal was completely consumed, in many parts of the sample during aging at 200 °C for 60 days and a Cu_3Sn IMC was formed at the consumed part (Fig. 22). The shear strength decreased significantly with increasing aging temperature and time. For aging at 185 °C for 15 days and at 200 °C for 3 days, fractures occurred in the bulk solder. For prolonged aging, fractures partially occurred at the $(Cu,Ni)_6Sn_5$ + Au/solder interface for aging at 185 °C and at the $(Ni,Cu)_3Sn_4$/Ni interface for aging at 200 °C (Fig. 23).

4.4. Electroless Ni–P

Electroless Ni–P deposition has found widespread use in the fabrication of under bump metallization (UBM) because it provides a transition to crystalline compound at 250 °C. It is a low maskless process used in electronic packaging especially in UBM for flip chip applications. Solid/solid interfacial reactions of electroless Ni–15%P with Sn–0.7Cu was investigated by Huang et al. [76] by performing thermal aging at 150 °C up to 1000 h. As-soldered Sn–0.7Cu/Ni–P (250 °C for 1 min) exhibited needle shaped $(CuNi)_6Sn_5$ IMC particles at the interface. The P enriched layer Ni_3P was observed in between the interfacial IMCs and Ni–P as shown in Fig. 24. With increase in aging time, the grains of $(CuNi)_6Sn_5$ IMC gradually coarsened into stout rods in morphology. The diameter of stout rods were found to be in the range of 0.5 to 2.5 μm as aged for 150 °C up to 1000 h (Fig. 25). The growth rate constant (k), for interfacial IMC layers and P-enriched layers (underneath) during aging at 150 °C was in the range of

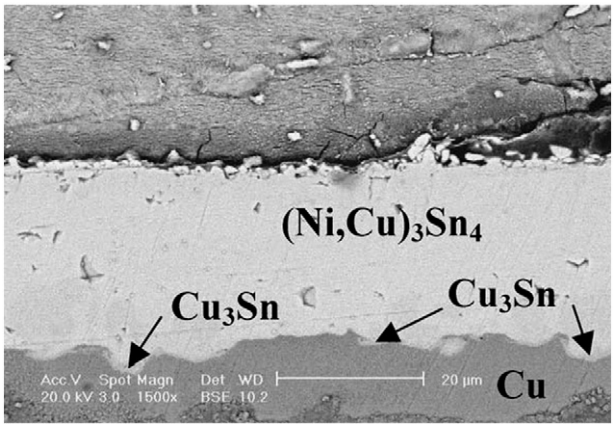

Fig. 22. SEM micrograph of the Sn–0.7Cu solder/Ni BGA joint aged at 200 °C for 60 days. [75].

8.79×10^{-9} m/s$^{1/2}$ (IMC layer) and 6.94×10^{-10} m/s$^{1/2}$ (P-enriched layer). Aging for 150 °C from 0 to 1000 h, the chemical composition of $(CuNi)_6Sn_5$ phase somewhat increased with increasing aging time, ranging from $(Cu_{0.63}Ni_{0.37})_6Sn_5$ to $(Cu_{0.55}Ni_{0.45})_6Sn_5$. The activation energy for the growth of $(CuNi)_6Sn_5$ IMC layer during initial aging was 70.3–82 kJ/mol and with increase in aging $(NiCu)_3Sn_4$ also formed at the interface. The activation energy for this layer was found to be 56.2 kJ/mol.

Cho et al. [77] also studied the interfacial reactions and evolution of microstructure and mechanical properties of Sn–0.7Cu after reacting with Ni–P UBM during thermal aging. For the as-reflowed samples, thin rod shaped IMCs were observed at the interface as shown in Fig. 26a. The IMCs formed at the Sn–0.7Cu solders/Ni–P UBM interface aged for a period of 1000 h were identified as Sn–Cu–Ni ternary phases, consisting of 45.8 at.% Sn, 42.7 at.% Cu, and 11.4 at.% Ni (marked as a "A" in Fig. 26b). During thermal aging at 150 °C for 1000 h, $(Cu,Ni)_6Sn_5$ IMCs are observed at the Sn–0.7Cu/UBMs interface (location A in Fig. 26b). Fig. 27a and b shows the optical micrographs of as-reflowed and aged (150 °C for 500 h) Sn–0.7Cu solder at a region far away from the interface. As-reflowed Sn–0.7Cu consists of β-Sn dendrites and eutectic phases (dark region, a mixture of intermetallic particles in β-Sn). After aging, the β-Sn dendrite cells disappeared, and many large IMC particles occurred in the Sn matrix. The IMC particles were coarsened compared to that at the as-reflowed condition. The shear strength of the reflowed Sn–0.7Cu ball/Ni–P was about 330 gF, 290 gF aged for 500 h and decreased to less than 300 gF

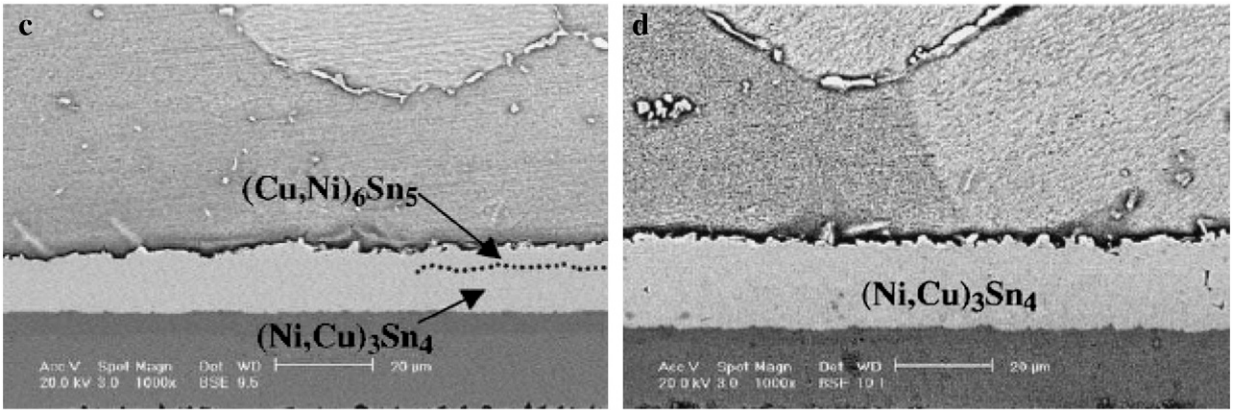

Fig. 21. SEM micrographs of the Sn–0.7Cu solder/Ni BGA joints aged at 200 °C for (c) 15 days and (d) 50 days. [75].

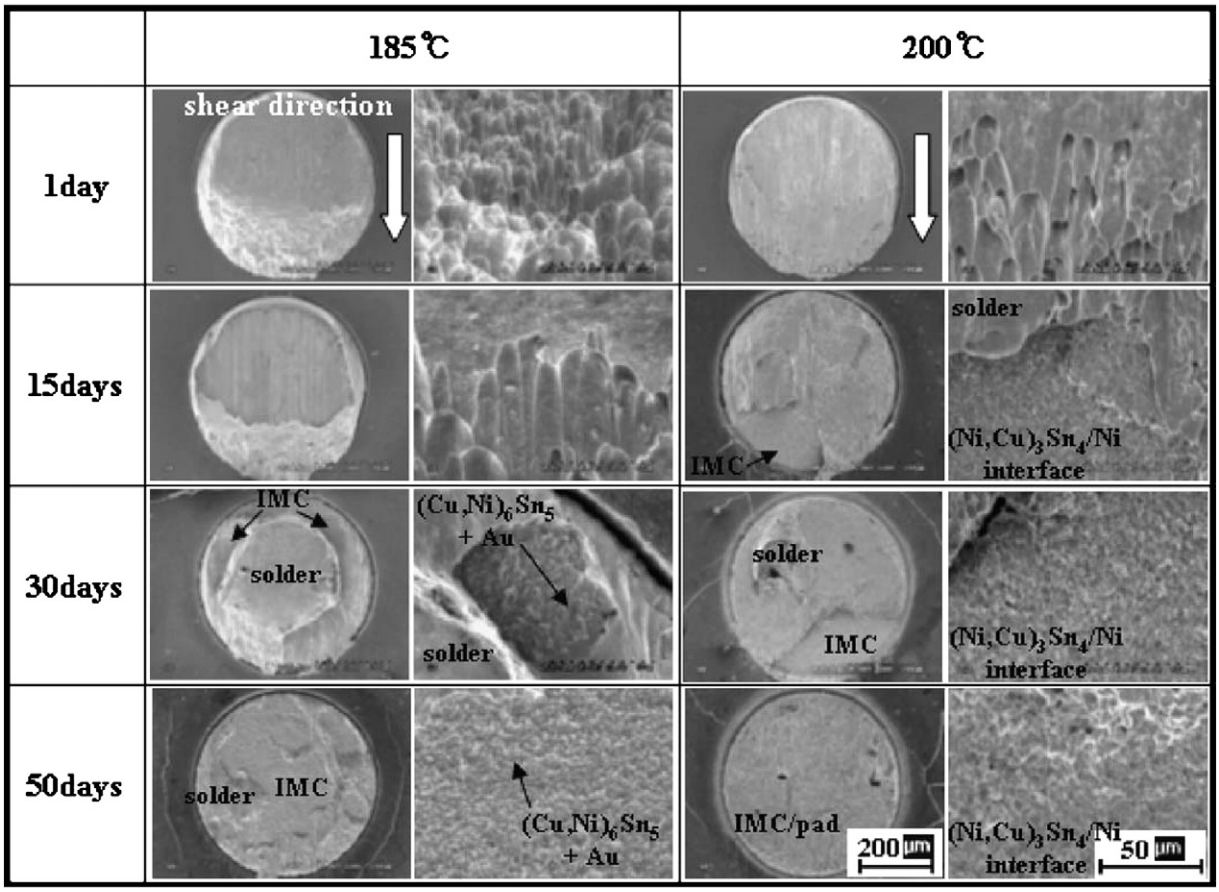

Fig. 23. The fracture surfaces of Sn–0.7Cu/Ni solder joints aged under different conditions.
[75].

after aging for 1000 h. Vickers hardness number (VHN) for the as-reflowed Sn–0.7Cu ball/Ni–P UBM was about 13.2 and VHN for aged sample at 150 °C for a period of 500 h was found to be 10.5.

4.5. Cobalt

The electromigration (EM) induced failure and degradation of joint strength are commonly observed in Cu based bond pads as extensive reaction between solder and Cu interface leads to massive interfacial Cu–Sn compound formation and serious Cu dissolution. Therefore, electroplated Ni and Ni(P) are frequently used on Cu-substrate, to prevent the rapid interfacial reaction between solder and Cu substrate/bond pad. It is well known that, Ni(P) layers cause some serious reliability issues like “black-pad” issue. Black Pad is an acute corrosion of the nickel plating layer, causing it to appear black in color. Hence, Co is a frequently used as a metal bond pad in electronic applications because solder/Co joints reveal superior mechanical joint

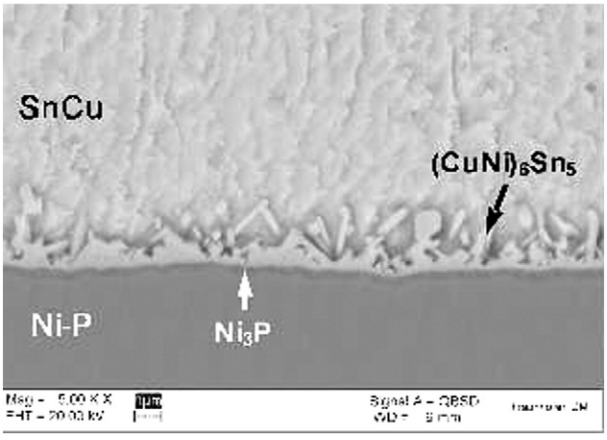

Fig. 24. Cross sectional view of the interfacial IMCs formed between Ni–P and the Sn–0.7Cu solder in as-soldered specimen (250 °C for 1 min).
[76].

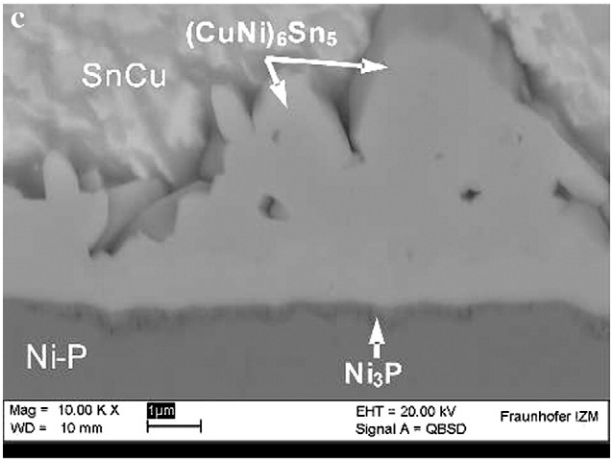

Fig. 25. Cross-sectional microstructure of the interfacial IMC layers in specimens after aging at 150 °C for 1000 h.
[76].

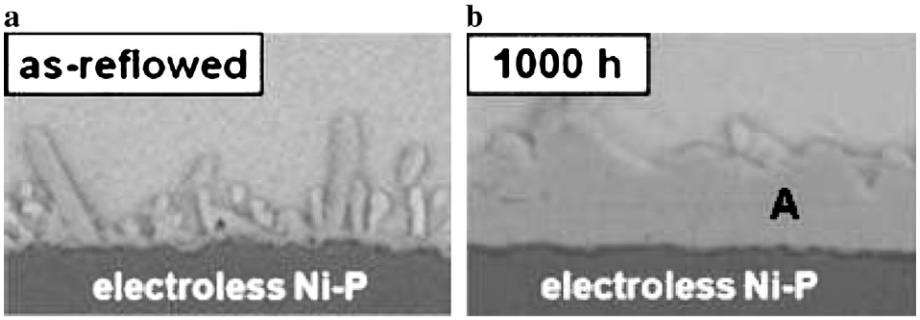

Fig. 26. Cross-section images of Sn–0.7Cu/Ni–P UBM (a) after reflow (b) aging at 150 °C for 1000 h. The location A was used to analyze composition by EPMA. [77].

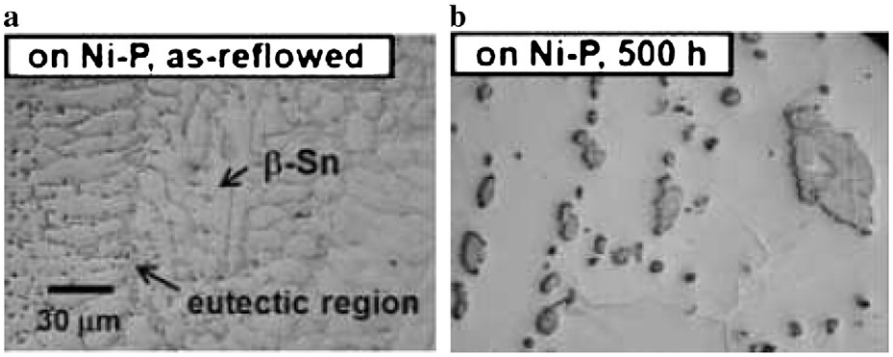

Fig. 27. Optical micrographs of Sn–0.7Cu solder taken far from the interface: (a) as-reflowed and (b) aged at 150 °C for 500 h. [77].

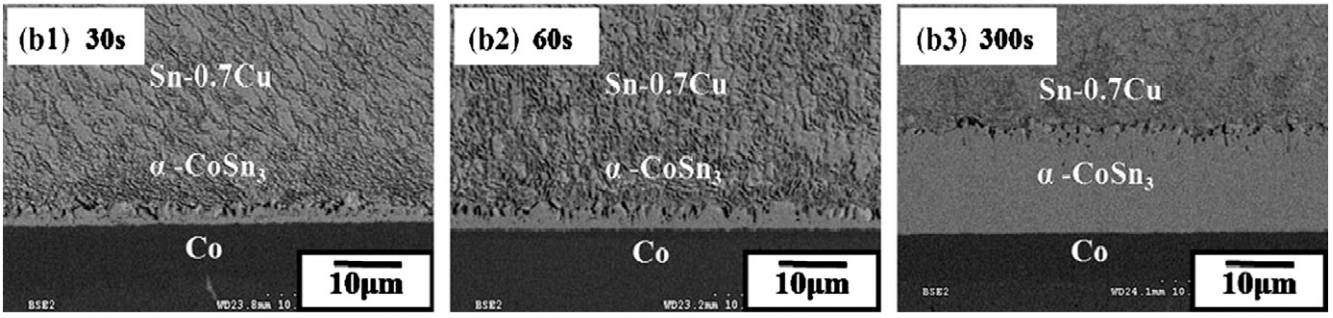

Fig. 28. SEM cross-sectional images of Sn 0.7Cu/Co samples for different reflow times at 250 °C. [78].

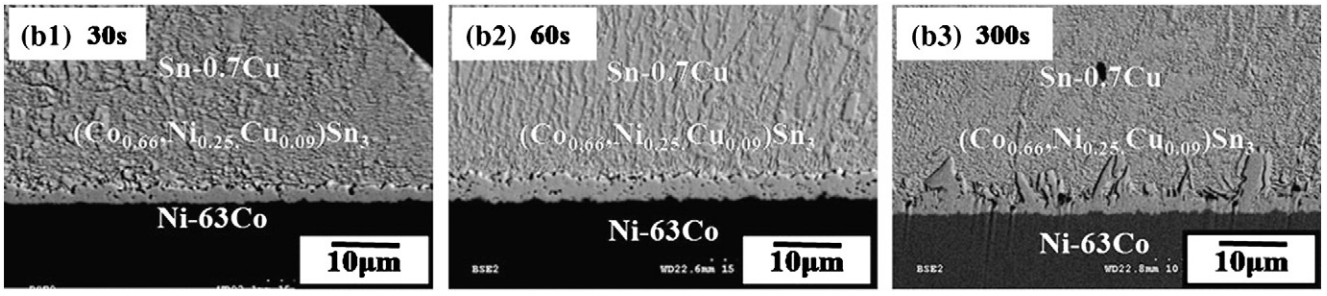

Fig. 29. SEM cross-sectional images of Sn–0.7Cu/Ni-63 at.% Co samples for different reflow times at 250 °C. [78].

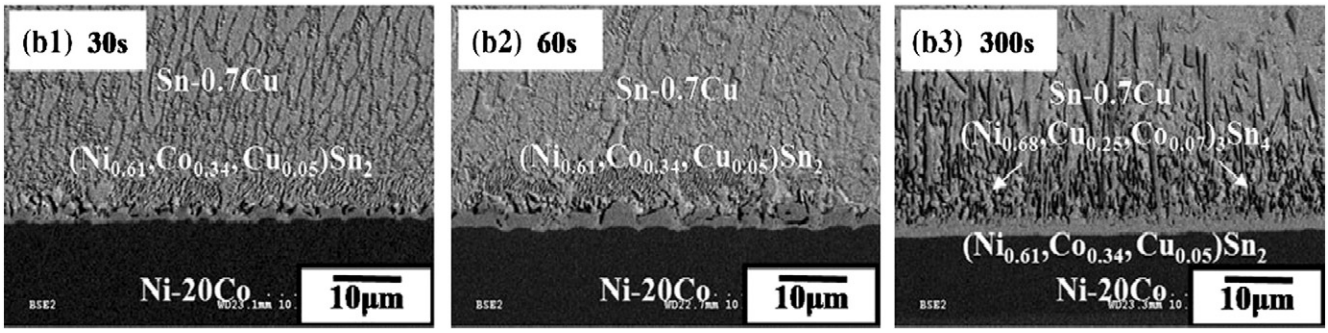

Fig. 30. SEM cross-sectional images of Sn–0.7Cu/Ni-20 at.% Co samples for different reflow times at 250 °C. [78].

Table 6
Chemical composition at Sn–0.7Cu/Cobalt, Ni–xCo interface. [78]

Solder	UBM/substrate	IMC phase
Sn–0.7Cu	Co	$(Co_{0.92},Cu_{0.08})Sn_3$
	Ni-63 at.% Co	$(Co_{0.66},Ni_{0.25},Cu_{0.09})Sn_3$
	Ni-20 at.% Co	$(Ni_{0.61},Co_{0.34}, xCu_{0.05})Sn_2 + (Ni_{0.68},Cu_{0.25},Co_{0.07})_3Sn_4$

strength and better wettability compared with the Ni(P) bond pad. It is also found that a rapid reaction could occur between the Sn rich solders and Co metal layers, resulting in a low-strength solder joint. Addition of Ni to the Co layer may possibly suppress the interfacial reaction between Sn rich solder and Co bond pad.

Huang et al. [78] have studied the interfacial reactions between Sn–0.7Cu/Cobalt and electroplated Ni–Co alloy layers at various reflow times. Figs. 28, 29 and 30 show cross-sectional SEM images of the Sn–0.7Cu/Co and Ni–xCo (x = 63 at.%, 20 at.%) samples after 30 s, 60 s, and 300 s of reflow at 250 °C. $CoSn_3$ was the only interfacial intermetallic compound formed at the Sn–0.7Cu/Co interfaces in spite of the Cu concentration and $(Co,Ni,Cu)Sn_3$ compound layers were observed at the interface of eutectic Sn–Cu solder/Ni-63 at.% Co. For solder/Ni-20 at.% Co, the $(Ni_x,Cu_y,Co_{1-x-y})Sn_2$ intermetallic compound layer formed early, after about 60 s of reflow. After extensive reflow (300 s), needle-like interfacial $(Ni_x,Co_y,Cu_{1-x-y})_3Sn_4$ phase formed above the continuous $(Ni_x,Cu_y,Co_{1-x-y})Sn_2$ compound layer. The chemical composition of the interfacial compound layers at the Sn–0.7Cu/Co and Ni–xCo interfaces as determined by EPMA is given in Table 6.

4.6. Platinum

Platinum as a base conductor is widely used in hybrid integrated circuits. Platinum metallization layer on integrated circuit was explored [79] because, platinum is highly resistant to oxidation and has a dissolution rate as low as nickel. Pt is a successful top surface layer for use in under bump metallurgy and also has acceptable properties as a wetting layer for industrial applications [80].

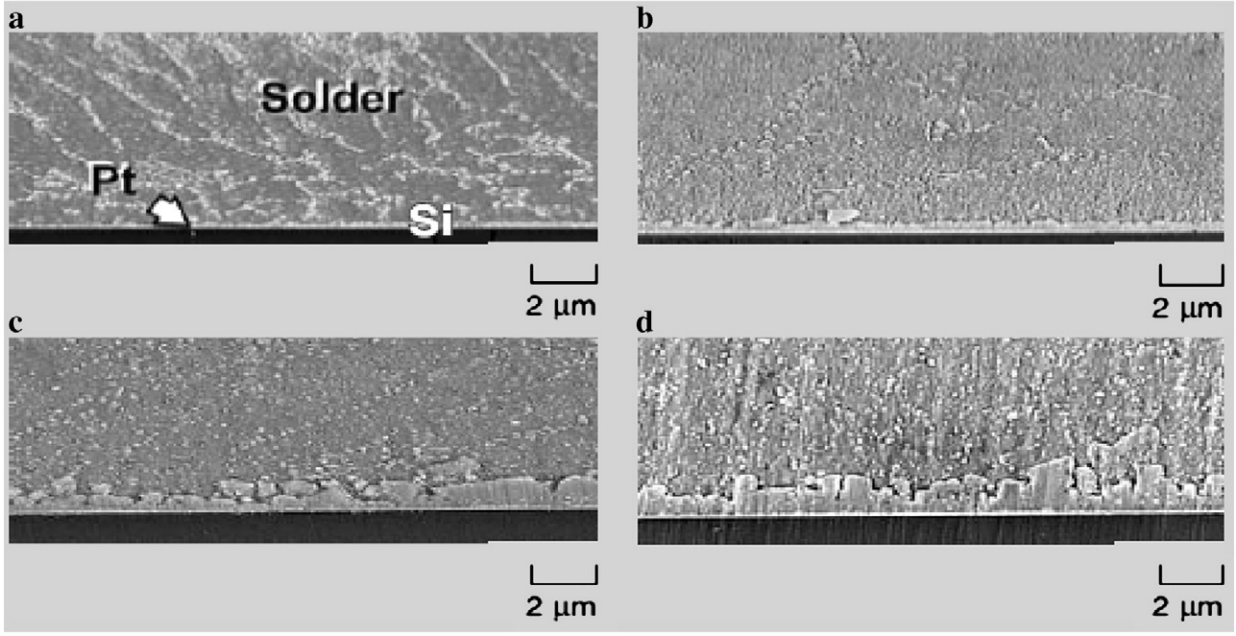

Fig. 31. Cross-sectional SEM images showing Sn–0.7Cu/Pt interfaces with various reflow times: (a) 30 s (b) 90 s (c) 360 s and (d) 600 s. [81].

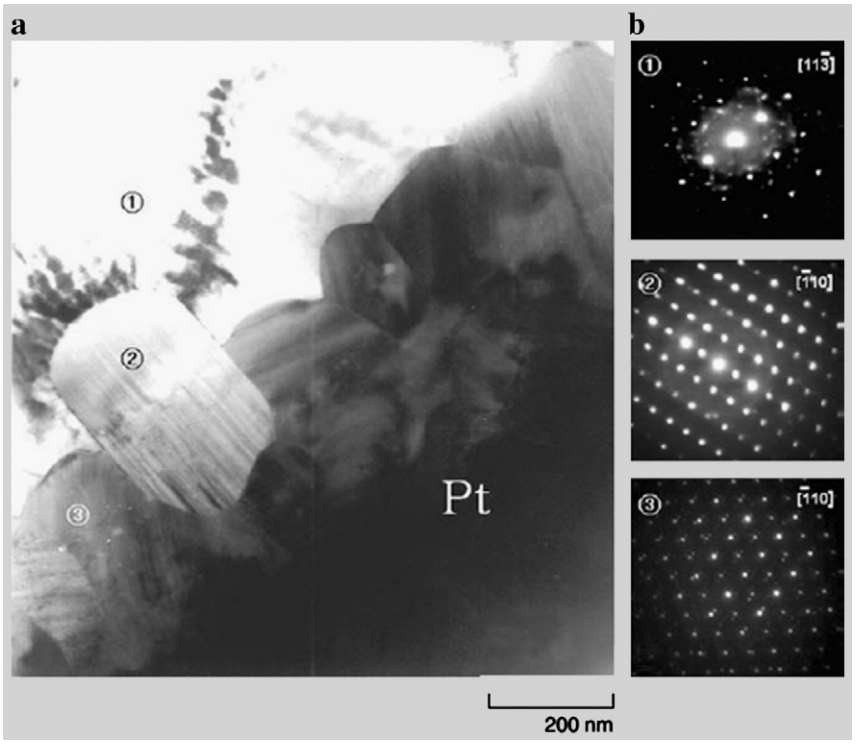

Fig. 32. (a) BF-TEM micrograph showing the Sn–0.7Cu solder/Pt interface after reflow at 260 °C for 30 s, and (b) SAD patterns obtained from grains 1, 2, and 3. [81].

Kim et al. [81] investigated the interfacial reaction of Sn–0.7Cu solder with platinum. Platinum (500 nm thick) deposited on silicon wafer was used as substrate material. Fig. 31 shows SEM images of the interfaces between Sn–0.7Cu/Pt substrate with various reflow times of 30 s, 90 s, 360 s, and 600 s at 260 °C. A continuous intermetallic layer was formed at the solder/platinum interface. The thickness of interfacial intermetallic, increased with reflow time. $PtSn_4$ intermetallic compound was found at the interface. Fig. 32 shows the TEM bright field (BF) image and selected area diffraction (SAD) patterns for an Sn–0.7Cu/platinum reacted at 260 °C for 30 s. The grains 2 and 3 between solder and platinum (as shown in Fig. 32.) were identified as the reaction product PtSn4 and the grain 1 corresponds to β-Sn. Even after the Sn–0.7Cu/Pt specimens were reflowed at 260 °C for 360 s, the grains grown from the platinum interface were identified as $PtSn_4$. The slow growth rate of $PtSn_4$ is a merit of platinum as a metallization layer, because the growth of $PtSn_4$ phase obeys the parabolic growth law. The parabolic growth kinetic behavior implies that interfacial IMC growth is controlled by bulk diffusion of elements to the reaction interface [81].

Table 7
Contact angle and Vickers microhardness for Sn–0.7Cu/Cu joint. [82]

Solder/substrate	Area of spread (mm^2)	Contact angle (θ)	Vickers microhardness (HV)
Sn–0.7Cu/Cu	32.17	21.65	16

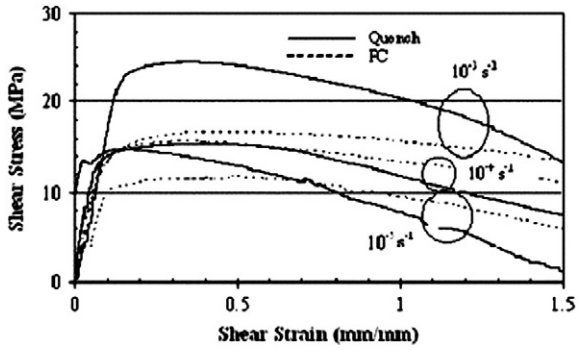

Fig. 33. The Sn–0.7Cu stress–strain curves comparing FC and QC specimens tested at three different strain rates. [83].

5. Mechanical properties of Sn–0.7Cu alloy

The microstructure and mechanical behavior of solders are very important because both affect the strength of the solder joint. The cooling/solidification rate of the solder has a significant effect on the microstructure and mechanical behavior of the solder [7]. Literature

Table 8
Ultimate shear strength (MPa) at room temperature for as-cast FC and QC eutectic Sn–0.7Cu samples. [83]

γ sec^{-1}	Cooling	Ultimate shear strength (MPa)
10^{-5}	QC	14.8 ± 0.01
	FC	11.5 ± 0.016
10^{-4}	QC	15.5 ± 0.01
	FC	15.6 ± 0.01
10^{-3}	QC	24.4 ± 0.011
	FC	16.6 ± 0.01
10^{-2}	QC	24.1 ± 0.006
	FC	24.2 ± 0.011
10^{-1}	QC	32.8 ± 0.005
	FC	31.6 ± 0.01

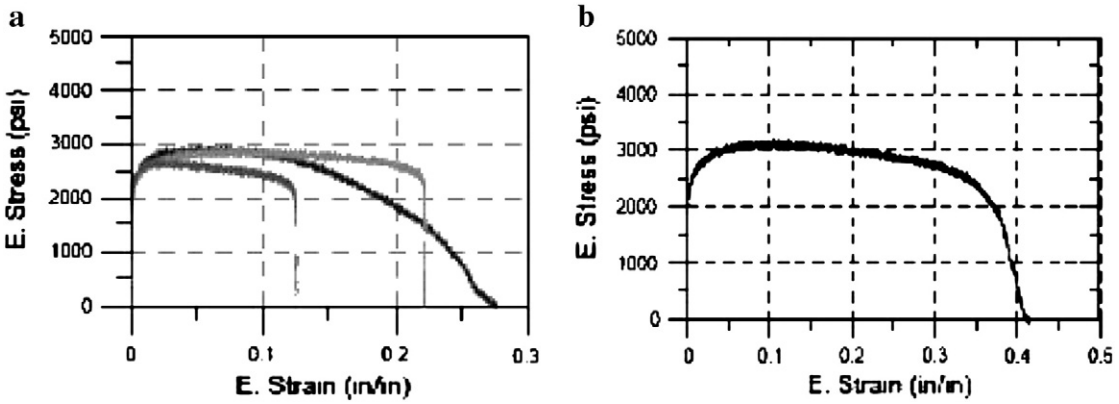

Fig. 34. Engineering stress–strain curves for the Sn–0.7Cu specimens. (a) Water-quenched (WQ) and (b) air-cooled (AC). [84].

review suggests that the kind of IMC formation at the interface is controlled by the diffusion rate/cooling rate of solders into the substrates. The measurement of the mechanical properties of the solder joint is much more difficult than bulk solders. For a given solder composition, volume of solder and joint geometry, method of joining will affect the solder joint properties. Solder characterization that includes the assessment of the type, strength, mechanical behavior and distribution of IMCs at the solder joint interface is important. The effects of aging and cooling rate on microstructure, mechanical properties especially shear strength, creep, tensile behavior and fracture toughness of Sn–0.7Cu solder are discussed in the following section.

Bae et al. [82] examined the microstructure and adhesion strength of the Sn–0.7Cu/Cu solder joint. The solder showed better wettability with a contact angle of about 22°. ε Cu_3Sn (3 μm thick) phase evolved just above the substrate. The shear strength of joint decreased linearly with increasing aging time after soldering at 290 °C for 10 min and after aging at 180 °C for 2 and 7 days. Table 7 gives the values of the contact angle and Vickers microhardness for Sn–0.7Cu/Cu joint.

As indicated earlier the cooling rate of the solder affects the solder microstructure and extensively influences the mechanical properties of the solder joint. In electronic applications the solder joints are subjected to shear stress during service. The effects of cooling rate and strain rate on the shear strength and mechanical properties of eutectic Sn–Cu were examined by Maveety et al. [83]. Two different cooling rates (quench cooling 50 °C/min (QC) and furnace cooling 2 °C/min (FC)) were adopted by the researchers to create large and fine grains, since the grain size can have an impact on mechanical strength. The shear testing was performed at room temperature at strain rates of 10^{-5}/s, 10^{-4}/s and 10^{-3}/s. Fig. 33 shows the stress–strain curves for Sn–0.7Cu for QC and FC samples tested at three different stain rates. It is found that the ultimate shear strength (UTS) increased with increase in strain rate. FQ samples have a larger impact on increasing the shear strength than QC samples, whereas the QC samples showed greater shear strength at higher strain rate than the FC sample. A strain rate of 10^{-3}/s produces higher work hardening in QC samples, whereas work hardening effect is low to moderate in the FC samples.

Table 9
Tensile properties for bulk water-quenched and air-cooled specimens of Sn0.7Cu alloy. [84]

Solder	Process	YS (psi)	UTS (psi)	Uniform elongation (%)	Total elongation (%)
Sn–0.7Cu/Cu	WQ[a]	2220	2820	5.4	20.8
	AC	2320	3130	9.1	41.2

[a] Indicates the average value of three trials (Fig. 34a).

Solders tested at room temperature, at five strain rates ranging between 10^{-5}/s and 10^{-1}/s are given in Table 8.

The study of casting of bulk Sn–0.7Cu solder with different solidification rates, water-quenched (WQ) and air-cooled (AC) and its mechanical properties have been measured from tensile tests and hardness testing [84]. The results of the tensile testing for Sn–0.7Cu solder alloys are shown in Fig. 34. A summary of the tensile properties is given in Table 9. It is observed that, there is not much difference in the tensile properties of the specimens processed at the two solidification rates. Therefore solder droplets with different cooling rates were produced by researchers [84] for comparison. Here the solder droplets were deposited on copper plates at 0 °C, 22 °C and 70 °C. The microstructures of the water quenched tensile specimens and solidified solder droplets were found similar to those obtained at slower cooling rates. This also corresponds to lower mechanical properties. The process of preparing bulk specimens for tensile testing revealed slow cooling rate compared to actual solder joints. These results indicated that, the procedure recommended by NCMS (National Center for Manufacturing Sciences) does not actually produce tensile test specimens with microstructure that can be compared with the actual solder joints generated at faster cooling rates. Therefore, Madeni et al. believed that the mathematical models developed to predict the performance of joints based on these data may not compare well with the actual solder joint performance.

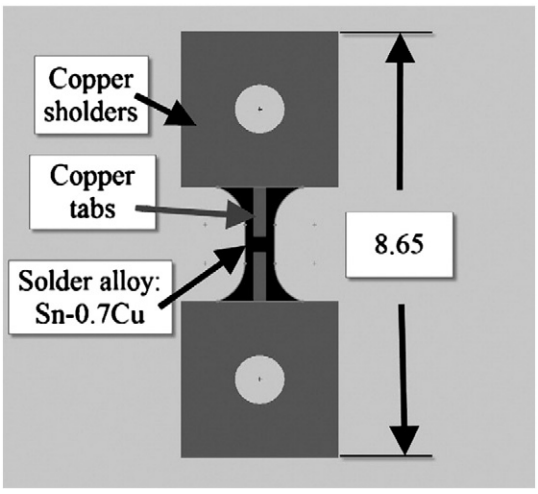

Fig. 35. A sketch of the miniature Sn–0.7Cu soldered specimen. [87].

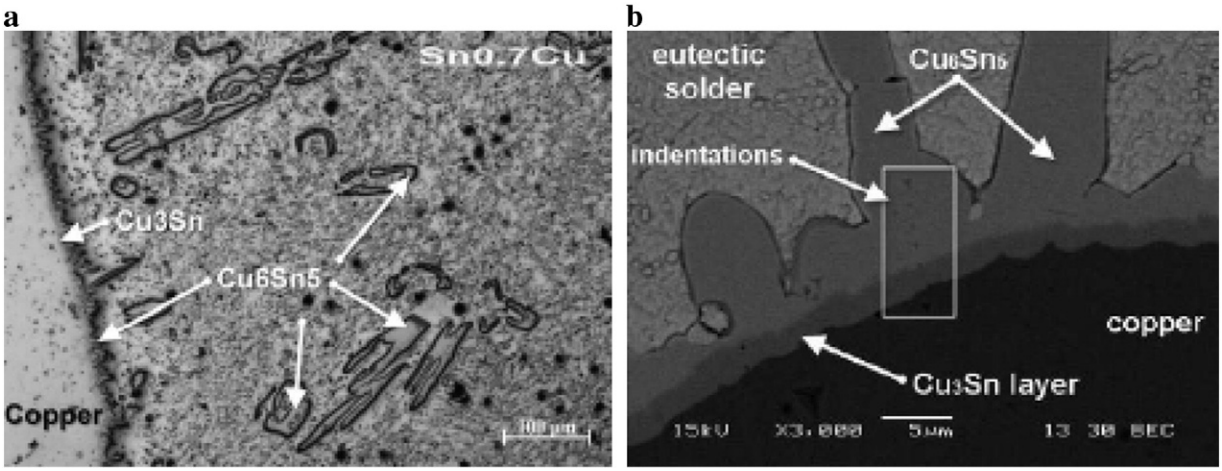

Fig. 36. (a) Microstructure of as-soldered miniature joint. (b) SEM micrograph of an aged miniature joint for 1000 h at 150 °C. [87].

In recent days nanoindentation techniques are widely used in the field of electronic applications in order to assess meticulously the mechanical response of the small volume soldered joints [85]. It distinguishes the confined mechanical behavior of a specific locality from the bulk response. Nanoindentation accurately measures the mechanical behavior of individual miniature solder components having area which may only be a few square micrometers or even nanometers and individual phases in lead-free bulk solders [86].

The mechanical testing and nanoindentation characterization of miniature Sn–0.7Cu lead-free solder joints components subjected to various metallurgical conditions and strain rates have been recently investigated by Rosenthal et al. [87]. Sn–0.7Cu miniature joints with Cu were tested at room temperature for two initial conditions: (a) as-soldered and (b) after aging at 150 °C for 1000 h in a capsule filled with inert gas. A sketch of the miniature Sn–0.7Cu soldered joint specimen is shown in Fig. 35.

As-soldered miniature soldered joint exhibited 5–10 μm thick Cu_6Sn_5 IMC layer, along the interface between Cu substrate and Sn–0.7Cu solder and a very thin layer of >1 μm Cu_3Sn IMC appeared between the Cu and the Cu_6Sn_5 IMC layer (Fig. 36a). After aging at 150 °C for 1000 h, the IMC Cu_3Sn was detected and the Cu_6Sn_5 showed some branches towards the eutectic solder (Fig. 36b). After performing nanoindentation measurements only a small increase in indentation modulus of aged specimens was observed as compared to as-soldered specimens. Table 10 gives the hardness (H) and modulus (E) values for as-soldered and aged miniature joints obtained from nanoindentation measurement. It is found that Cu_3Sn IMC layer with extensively higher indentation modulus and hardness contributed only to the interface quality and not to the overall strength of the soldered joint. This IMC phase is not brittle and it is not a site for nucleation of voids and cracks. Rosenthal et al. [87] suggested that both tensile and nanoindentation testing can serve as a good quality, fairly responsive method to determine mechanical behavior of phases in miniature Pb-free soldered joints.

Table 10
Hardness (H) and indentation modulus (E) values for as-soldered and aged samples obtained from nanoindentation measurement. [87]

	Nanoindentation site	E (GPa)	H (GPa)
As-soldered	Cu_6Sn_5: interface scallop	129 ± 4.0	5.6 ± 2.1
	Cu_6Sn_5: precipitate in eutectic solder	89 ± 2.2	4.8 ± 1.9
	Eutectic solder	42 ± 6.0	0.3 ± 0.1
Aged, 1000 h at 150 °C	Cu_6Sn_5: interface scallop	133 ± 9.0	6.2 ± 1.9
	Cu_3Sn: layer between the substrate and the Cu_6Sn_5 layer	148 ± 5.0	7.2 ± 0.3
	Cu_6Sn_5: precipitate in eutectic solder	93 ± 1.0	4.8 ± 2.0
	Eutectic solder	52 ± 6.0	0.4 ± 0.1

The unified constitutive models for solders have been reported since 1982 and a lot of work also has been carried out on cyclic constitutive models. However, none of these research works are directed towards uniaxial ratcheting of lead-free solders. Bai and Chen [88] successfully simulated the loading/unloading asymmetry phenomenon in uniaxial ratcheting tests with good predicting results.

Bai's [88] novel unified model with back stresses (short range back and long-range back stress) concept was used to simulate the uniaxial tensile test data on Sn–0.7Cu solder. Short range back stress means those processes having fast kinetics and processes with slower kinetics represented long-range back stress. All the uniaxial tensile curves congregate jointly on a master curve and look similar if both the stress and strain are divided by saturation stress (Fig. 37), which indicated that all the tensile curves follow the same evolution rule. The only discrepancy between them is just the saturation stress. Thus, based on this observable fact, the stress–strain curves with varied temperatures and strain rates can be "unified" using the concept of

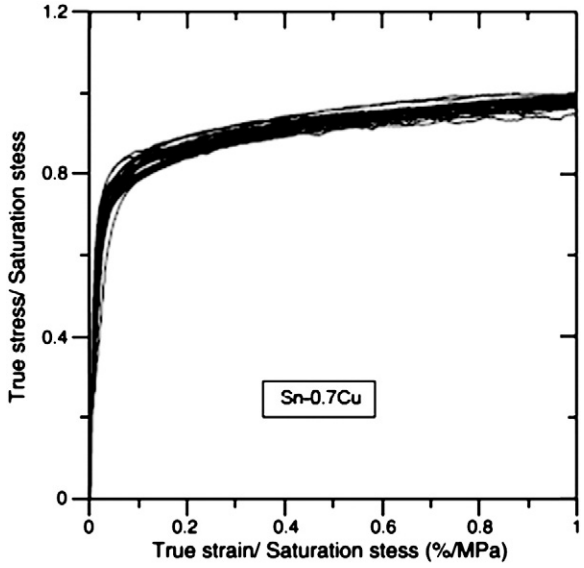

Fig. 37. True stress/saturation stress vs. true strain/saturation stress for Sn–0.7Cu. [88].

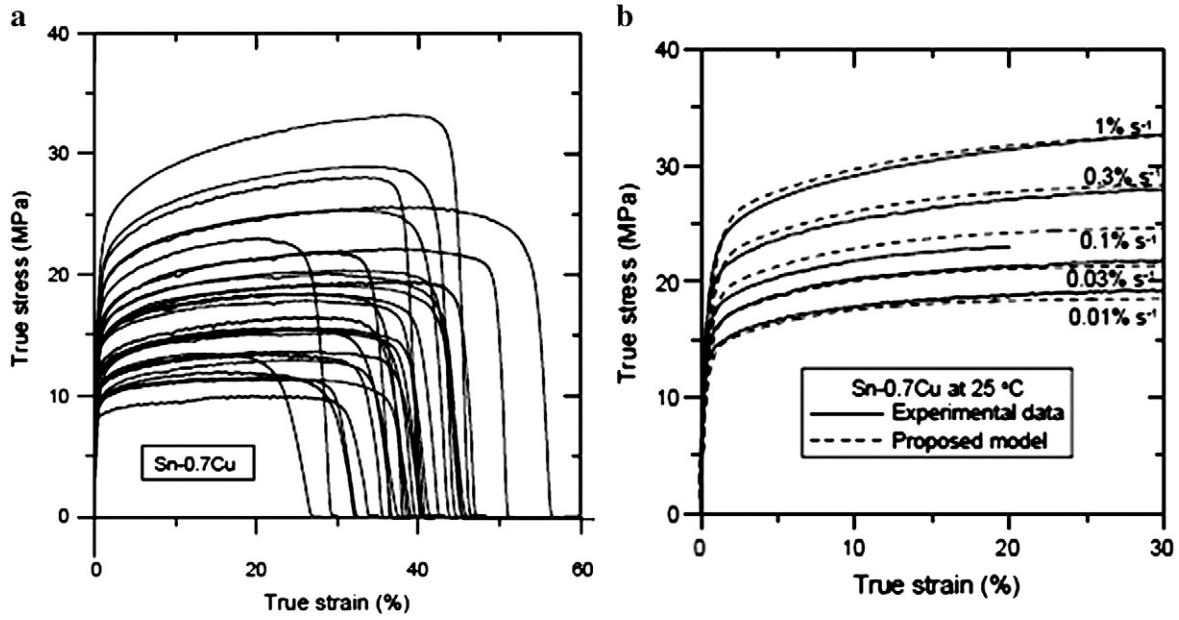

Fig. 38. (a) The uniaxial tensile test curve of Sn–0.7Cu. (b) Simulation of uniaxial tensile test for Sn–0.7Cu by proposed model at 25 °C. [88].

"saturation stress". If one curve has been described successfully, then other curves can be simulated as well [88].

Most constitutive old models for solder alloys separated the inelastic deformation into plasticity and steady state creep. In reality, it is generally complicated to separate the plastic strain from creep strain to find out the parameters of a separated model based on the mechanical experimental tests. Hence, a unified constitutive relation was proposed by Bai to describe "plasticity" and "creep" in the same equation.

A series of uniaxial tensile tests were performed by the researchers [88] with a number of different strain rates (1×10^{-4} to $1\times10^{-2}\ s^{-1}$) and temperature conditions (25 °C to 150 °C). Also two step strain rate jump test, three step short term creep test with stress jump and uniaxial ratcheting tests under cyclic loading were conducted by the researchers. Fig. 38a and b shows the uniaxial tensile and simulation of uniaxial tensile test for Sn–0.7Cu.

Stress–strain relation in uniaxial tensile tests is derived from the two back stresses using Eq. (3).

$$\sigma = \sigma^{*}Ko + K_s\sigma^{*} - K_s\sigma^{*}\left[1-\frac{(1-a)h_s\varepsilon_p}{K_s\sigma^{*}}\right]^{\frac{1}{1-a}} + K_1\sigma^{*}\left[1-\exp\left(-\frac{h_1\varepsilon_p}{K_1\sigma^{*}}\right)\right] \quad (3)$$

The material parameters of the new model for the Sn–0.7Cu solder determined by this model equation, where values of four parameters, h_s, K_s, a and h_l can be obtained from uniaxial tensile curve by a nonlinear least square fit. Table 11 gives material parameters of Sn–0.7Cu calculated from the proposed model, where σ, σ*, A, ε_p, and B are actual stress, saturation stress, material constant, inelastic true strain rate, and temperature factor respectively. K_o is over stress proportion coefficient (a material constant), h_l is long-range back stress evolution coefficient, K_l is long-range back stress proportion coefficient and 'a' is a material parameter.

The microstructural inhomogeneity and the stress concentrations in the solder joint contribute severely to the occurring fatigue damage. Experiments and common observations show that damage starts at and propagates along solder/substrate interfaces.

Reliability of the solder joints must be assessed through numerical simulation during the design process. Concerning the small sizes of solder joints, the numerical models should include the microstructure. The interface damage can be modeled using a cohesive zone approach or the cohesive zone modeling (CZM). CZM approach has been considered as a simple and feasible analytical tool for nonlinear fracture processes such as crack initiation, large-scale yielding condition, or irreversible unloading because it provides the ability to account for problems which are quite difficult to deal with by the linear elastic fracture mechanics [89,90].

In the cohesive zone formulation, traction 'T' is a linear function of the separation Δ whereas the energy dissipation associated with the gradual degradation of the material, is accounted for by the incorporation of a nonlinear damage variable D_α, which varies between zero (0) for damage-free and one (1) for completely damaged cohesive zones. A damage variable is introduced for the accumulation of damage throughout the cycling process described by an evolution law based on the formulation of Roe and Siegmund [89]:

$$T_\alpha = k_\alpha(1-D_\alpha)\,\Delta_\alpha \quad (4)$$

$$\dot{D} = C_\alpha\left|\dot{\Delta}\right|(1-D_\alpha + r)^m\left\langle\frac{|T_a|}{1-D_a}-\sigma f\right\rangle \quad (5)$$

Table 11
Material parameters of Sn–0.7Cu solder obtained from stress–strain model proposed by Bai and Chen. [88].

Solder	A (s^{-1})	m	B(K)	h_s (MPa)	K_s	a	h_l (MPa)	K_l
Sn–0.7Cu	365.41	0.126402	−164.131	30078.8	0.25	1.87670	78.9157	0.25

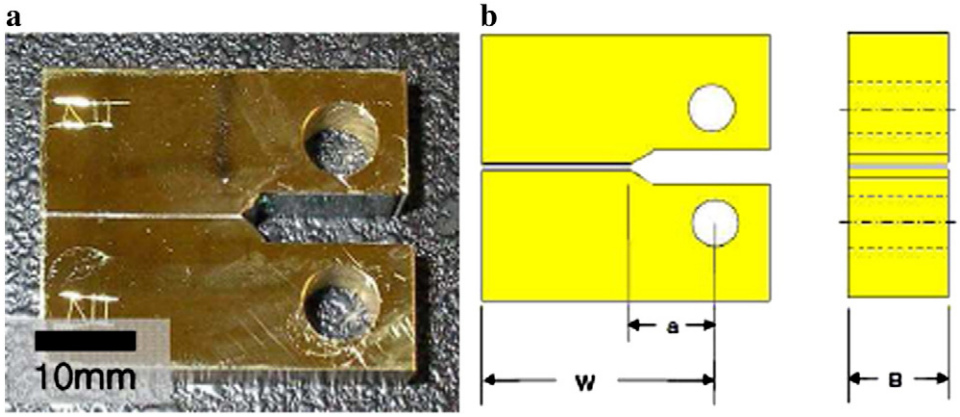

Fig. 39. (a) Macro view of CT specimen. (b) CT specimen for the measurement of interfacial fracture toughness W = 2.54 cm, B = 0.953 cm and a = 0.8 cm. [92].

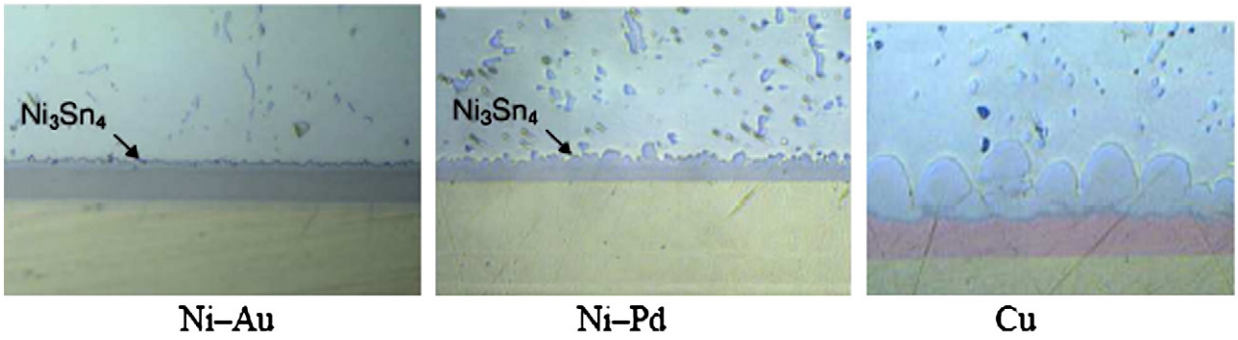

Fig. 40. IMC morphology observed on Ni–Au, Ni–Pd (after 45 s reflow) and Cu metallization for both Sn–0.7Cu solder (after 180 s reflow). [92].

[90,91] where 'k_α' is the initial stiffness of the cohesive zone, 'C_α' is a constant, which controls the damage accumulation, 'Δ_α' is the rate of the relative opening of the cohesive zone, 'r' and 'm' are constants which control the decay of the reaction force at the final stage of damage and 'σ_f' is the cohesive zone fatigue limit. Macauley brackets are used to prevent damage growth when the traction is below the fatigue limit.

Individual fatigue tests are simulated by the finite element method. Cohesive zones are located at interfaces where failure is observed. After a number of cycles, damage evolves at the bonding interfaces. The peak stress thus decreases with successive cycles.

Fracture toughness of the solder is very important property. It is measured using a compact tension (CT) geometrical specimen. The presence of IMCs is essential to promote a proper bonding and adhesion between the substrate and the solder. However, the existences of higher thicknesses particularly above 5–10 μm, of the intermetallic layer drastically decrease the fracture toughness of the joint [92]. The determination of the fracture toughness of the solder is very crucial for assessment of reliability of the solder joint system.

Hayes et al. [92] evaluated the relationship between the intermetallics formed during reflow (45, 90 and 180 s), their fracture behavior, and the resulting solder joint fracture toughness in Cu and Ni–Au and Ni–Pd metallization for Sn–07Cu alloy. Fig. 39a and b shows the macro view of compact tensile (CT) specimen after polishing and dimensions of the CT specimen respectively. (Ni, $Cu)_3Sn_4$ IMC was observed at interface of Sn–0.7Cu solder/Ni–Au and Ni–Pd substrates. But $(Ni,Cu)_3Sn_4$ IMC was coarser at the Ni interface for Sn–0.7Cu/Ni–Pd (Fig. 40). Sn–0.7Cu solder formed the characteristic continuous and relatively regular Cu_6Sn_5 and Cu_3Sn intermetallics when reflowed on copper for 45 s.

Increasing the reflow time to 90 s resulted in coarsening and thickening of the Cu_6Sn_5 layer. After 180 s of reflow, the Cu_6Sn_5

Table 12
Apparent fracture toughness (K_Q) of solder joints on Ni metallization. [92].

	Reflow time s	Fracture toughness MPa $m^{1/2}$
Sn–0.7Cu/Ni–Pd	45	9.13
	180	8.19
Sn–0.7Cu/Ni–Pd	45	Ductile failure
	90	9.23
	180	7.55

Table 13
Calculated values of Young's modulus. [93].

Phase/solder	Density $\times 10^3$ (kg m^{-3})	Young's modulus (GPa)	Resistivity $\times 10^{-8}$ (ohm.m)
Cu_6Sn_5	8.28	85.56	17.5
Sn–0.7Cu		64.1	11.14
		63.96 (matrix)	11.1 (matrix)

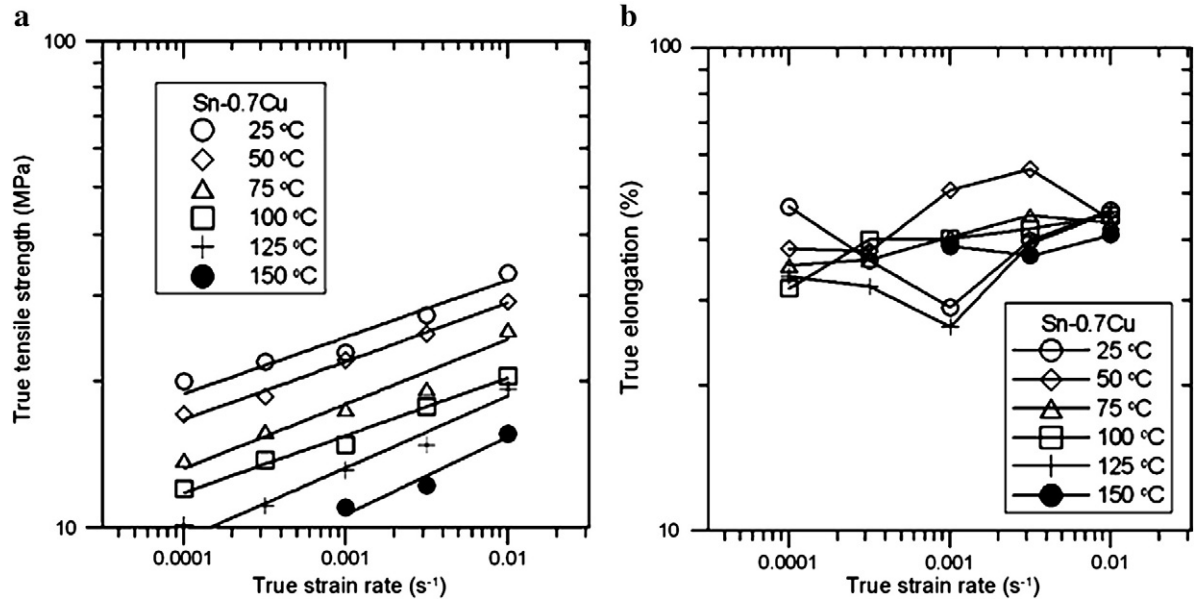

Fig. 41. (a) True tensile strength and (b) true elongations for Sn–0.7Cu at different strain rates. [95].

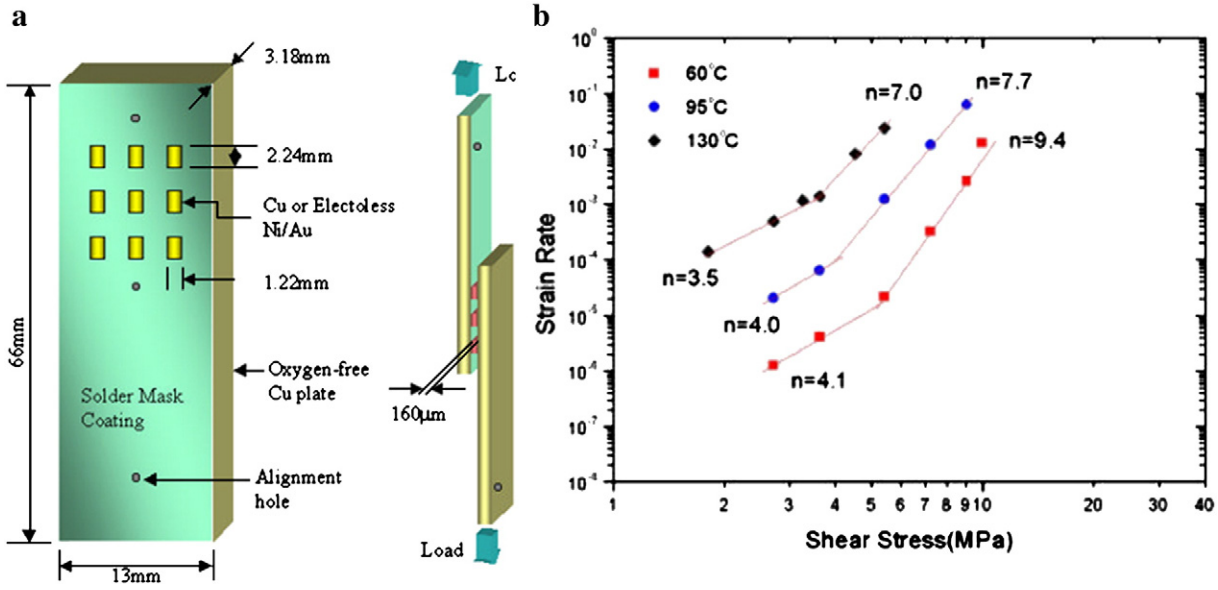

Fig. 42. (a) The creep specimen geometry. (b) Log–log plot of the steady-state strain rate vs. stress for Sn–0.7Cu solder joints. [96].

continued to become even coarser (Fig. 40c). The critical thickness (1.5–2.5 μm) of Ni_3Sn_4 tends to cause more failure within the IMC instead of bulk of the solder. The critical thickness for the identical effect for Cu_6Sn_5 was found to be approximately 6 μm. The apparent fracture toughness (K_Q) of Cu_6Sn_5 appeared to be greater than that of Ni_3Sn_4. Comparing with Ni_3Sn_4, Cu_6Sn_5 showed more rapid growth with increasing reflow time, resulting in significant decrease in toughness. Apparent fracture toughness (K_Q) of Sn–0.7Cu solder joints investigated by the researchers is given in Table 12.

The relation between valency, axial ratio(c/a),Young's modulus and resistivity of rapidly solidified eutectic Sn–Cu was investigated by

Table 14
Best-fit stress-exponents and activation energies for Sn–0.7Cu alloy. [96].

	n		Q(kJ/mol)	
	Low τ/G	High τ/G	Low τ/G	High τ/G
Sn–0.7Cu joint connecting Cu/Ni–Au substrate	Low τ/G 3.5	High τ/G 8.9	Low τ/G 90	High τ/G 85

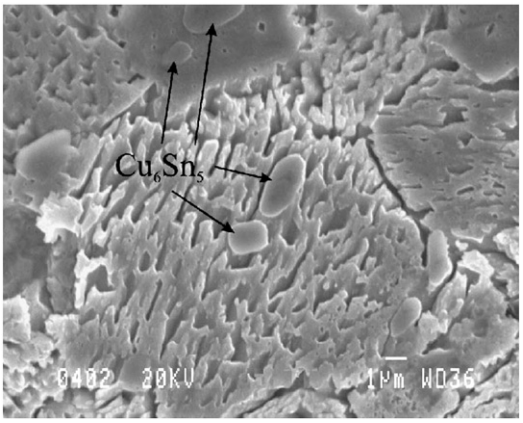

Fig. 43. SEM microstructure after aging at 150 °C for 20 h Sn–0.7%Cu. [98].

Ashram [93]. Using melt-spinning technique, eutectic alloy of Sn–Cu was produced. X-ray diffraction analysis (XRD) was also carried out to find axial ratios (c/a), where c and a are the lattice parameters. Using the rule of mixtures equation, Young's modulus of solder alloy was calculated, as given by equation

$$E_{alloy} = V_\alpha E_\alpha + V_\beta E_\beta \quad (6)$$

where V_α and E_α are the volume fraction and the Young's modulus of α phase. V_β and E_β are the volume fraction and the Young's modulus of β phase. It has been observed by the researchers that Young's modulus increases by increasing the axial ratio and decreases by decreasing it [93]. Adding Sn with low valency metals such as Cu increases the axial ratio. The resistivity decreases by increasing the axial ratio. The calculated value of Young's modulus of the matrix using this technique for the second phase is given in Table 13.

Microhardness (HV) of as quenched melt spun Sn–Cu eutectic alloy was measured. It is found that HV decreases by increasing the dwell time. For the alloy, HV has the lowest value (196.21 MPa), which is nearly constant up to 50 s, and then it decreases by increasing the time to 150 MPa for 90 s of indentation. For the same eutectic alloy, the melting temperature was found to be 227.4 °C ± 0.5 °C and the enthalpy of fusion is 48.2 kJ kg^{-1} ± 0.7 kJ kg^{-1} [94]. The effect of strain rate and temperature on the tensile properties of Sn–0.7Cu solder alloy at various strain rates (1×10^{-4} s^{-1} to 1×10^{-2} s^{-1}) was investigated by Bai [95]. The relationship between tensile strength and strain rate for solder alloy was described by the equation $\sigma = C\dot{\varepsilon}^m$, where σ is the tensile strength, $\dot{\varepsilon}$ is the strain rate, m is the strain rate sensitivity, and C is a constant. Fig. 41a shows the true tensile strength of the alloy indicating that strain rate sensitivity 'm' is relatively stable over the temperature range. The effect of temperature on the strain rate sensitivity 'm' is found to be very small. The activation energy for the creep of Sn–0.7Cu is found to be 27.3 kJ/mol and the ductility of alloy is independent of the strain rate or temperature (Fig. 41b).

The understanding of creep behavior and creep mechanisms is essential for the design of reliable joints because solder will deform at high-temperature creep, and solder joints finally fail by creep fatigue. The creep behavior of Sn–0.7Cu was investigated by making thin joints connecting Cu and Ni/Au metallized substrates. Fig. 42a shows the specimen geometry [96]. The Dorn equation (Eq. (5)) was used to find the creep behavior over temperature regime. The equation is written as

$$\gamma = \frac{AGb}{kT}\left[\frac{\tau}{G}\right]^n \exp\left[\frac{-Q}{kT}\right] \quad (7)$$

where, 'γ' is the shear strain rate, 'τ' is the shear stress, 'G' is the shear modulus, 'b' is the Burgers vector, 'Q' is the activation energy, 'k' is the Boltzmann constant and 'T' is the temperature. In high-stress regime the stress exponent (n) is about 7 for the alloy at 130 °C, but increases considerably as the temperature is decreased from 95 °C to 60 °C (Fig. 42b). This is due to the Sn-rich constituent itself. The best-fit

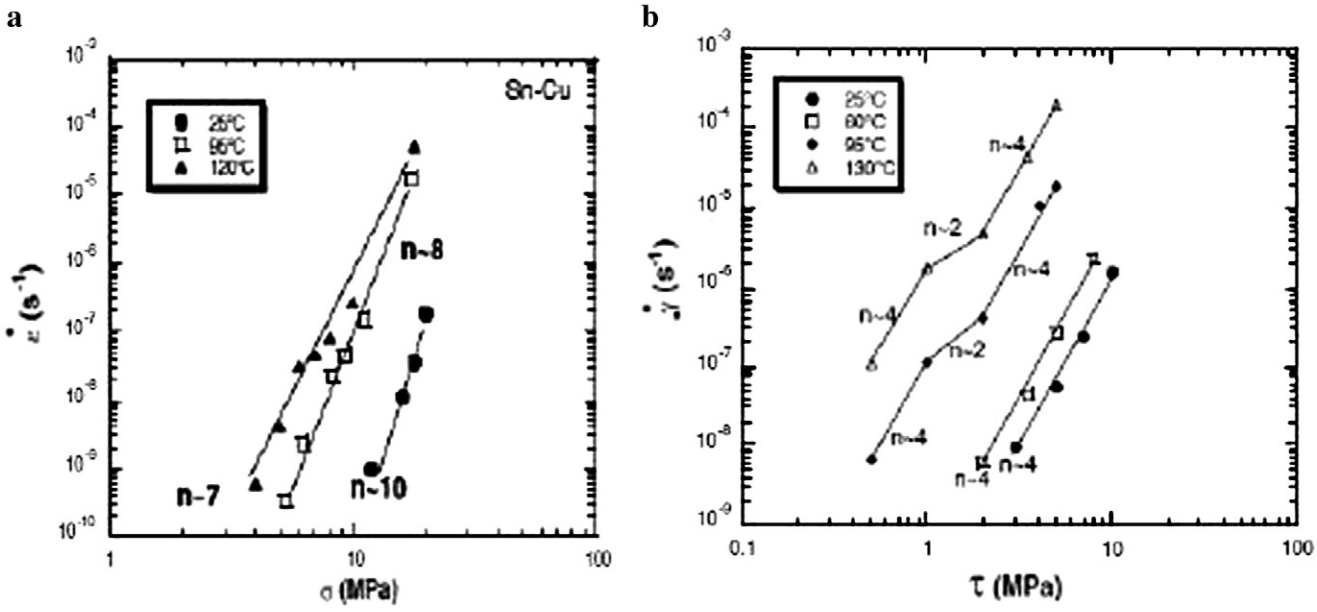

Fig. 44. (a) Steady-state creep rate as a function of stress for alloys cooled at 0.1 °C/s for bulk solder. (b) Strain rate vs. applied stress for solder joint showing S shape. [99].

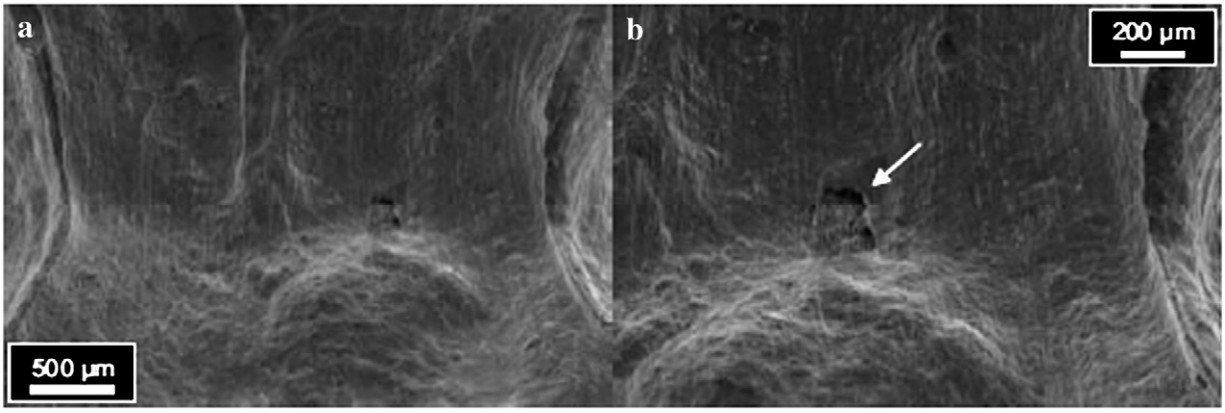

Fig. 45. Sn–0.7Cu specimen tested in impact at −125 °C: no fracture. (a) The specimen has essentially deformed plastically during testing, (the formation of stretch marks). (b) The specimen surface showing the occasional distraction of material continuity (arrow).
[102].

stress-exponents and activation energies obtained for Sn–0.7Cu are given in Table 14.

Huang [97] also investigated the creep resistance in relation with microstructure of bulk Sn–0.7Cu alloy. The creep tests were performed at 303 K (30 °C), 348 K (75 °C) and 393 K (120 °C) under various constant loads. For the eutectic Sn–Cu alloy the steady-state creep rates decrease with increasing volume fraction of precipitate Cu_6Sn_5 phases. The creep life of Sn–0.7Cu at 17.5 MPa and 348 K was found to be 0.175 h. The values of apparent stress exponents (n_a) at 30 °C, 75 °C and 120 °C were found to be 11.5, 9.8 and 7.3 respectively and attain higher values with increasing volume fraction of precipitated phases at the constant temperature, and with the decreasing temperature for the solder alloy.

Wu [98] also investigated the microstructure correlation with mechanical property for solder alloy aged at 150 °C for 20 h. After aging of the Sn–0.7%Cu alloy, coarse Cu_6Sn_5 particles (> than 2 μm in

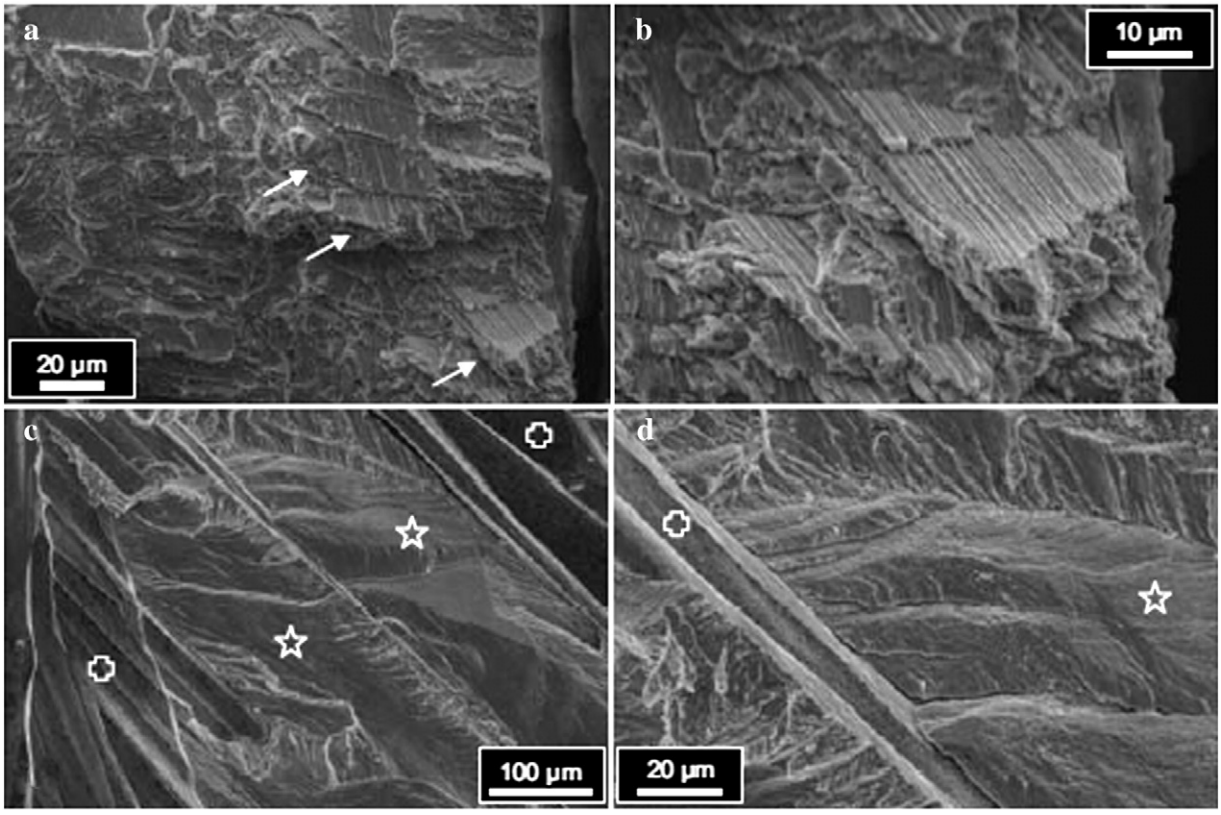

Fig. 46. Sn–0.7Cu specimen tested in impact at −135 °C. Primarily brittle fracture: a and b. Cleavage-like fracture of Sn: c and d. Areas characterized by intergranular separation (stars). (a) Part of the fracture surface with many ledges (arrows) formed during the cleavage-like failure of Sn. (b) Closer inspection of one of the ledges in (a); (c) part of the fracture surface revealing areas of intergranular fracture (crosses) separated by areas of transgranular fracture (stars). (d) Closer inspection of the border between intergranular (cross) and transgranular (star) fractures.
[102].

size) were dispersed at the grain boundaries and in the β-Sn grains (Fig. 43). But the dispersion of the particle precipitates in the microstructure was not uniform. The coarsening of particles was due to atomic diffusion and the accumulation of small Cu_6Sn_5 particles at high temperature. A more homogeneous microstructure with Cu_6Sn_5 particles dispersed within some grains of β-Sn and at grain boundaries was observed. An ultimate tensile strength (UTS) of about 30 MPa and extensive elongation was obtained for the Sn–0.7Cu alloy.

Creep behavior of bulk and small scale solder joint of eutectic Sn–Cu alloy was investigated by Sidhu et al. [99]. The bulk solder creep nature was controlled by subgrain formation of dislocations, pinned by grain boundaries and Cu_6Sn_5. The values of creep-stress exponents (n) were found to be in the range of 7 to 8 (Fig. 44a). The creep behavior of Sn–0.7Cu/Cu joint showed S shaped phenomenon (Fig. 44b) at high temperature, indicating that creep is accommodated by viscous grain boundary sliding.

The damage of Sn based solder joint is mainly caused by the cyclic deformation and creep of solder material and failure/ultimate fracture of Sn based solder joint are characterized by the formation of a coarsened band along which a main crack forms during thermomechanical fatigue. Grain boundary sliding is known to occur when boundaries are high angled, and is used as an advantage in superplastic forming [100]. Grain boundary sliding has been identified as a major precursor to damage in lead-free solder joints.

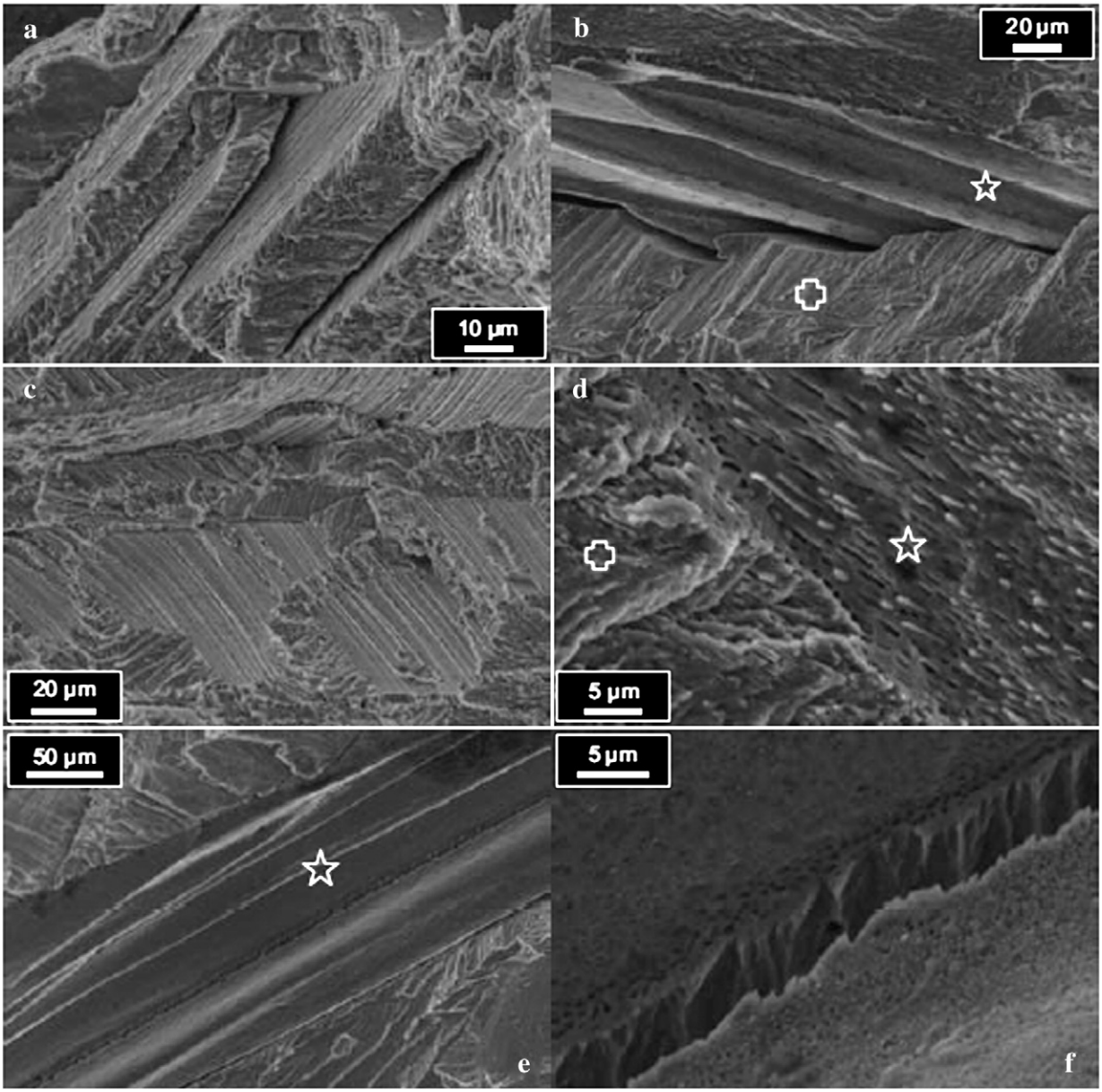

Fig. 47. Sn–0.7Cu specimens tested in impact at −155 °C [(a) and (b)] and at −170 °C [(c)–(f)]. (a) Brittle failure. (b) Apart from the cleavage-like failure of Sn (cross), areas of intergranular separation of Sn–Cu_6Sn_5 eutectic grains (star) occupy a large part of the fracture surface (c) Brittle failure: the extensive cleavage-like failure of Sn indicates severe embrittlement. (d) Close inspection of the border between an area of cleaved Sn (cross) and a Sn–Cu_6Sn_5 eutectic grain (star). The fibrillar phase in the eutectic consists of ultra-fine rods of Cu_6Sn_5 IMC. (e) Part of the fracture surface with obvious intergranular fracture (star) occurring between grains of the Sn–Cu_6Sn_5 eutectic. (f) Closer inspection of the interface between two adjacent Sn–Cu_6Sn_5 eutectic grains.
[102].

The main causal mechanism of damage of Sn based solder joint is attributed to the localization of plastic deformation that produces excessive crystal defects (dislocations, vacancies etc.), thus providing an additional driving force for atomic diffusion and therefore microstructural change (coarsening). However, the grain boundary sliding occurs during creep at elevated temperature (texture is unchanged) permitting larger amounts of strain accommodation. Even thermomechanical fatigue also causes grain boundary sliding. Sliding may be both a positive and negative effect, possibly delaying fracture in contrast to room temperature creep. Subgrains form in a manner dependent on the most active slip systems, and as the misorientations increase to near-coincident site lattice (CSL) conditions, they begin to slide [101]. The boundary sliding does not take place along a sharp interface [100].

Solder embrittlement is common in electronic applications. The impact trustworthiness of lead free solders is compromised when the service temperature decreases due to the ductile-to-brittle transition in the fracture behavior of β-Sn. The embrittlement of β-Sn occurs in the solder bulk, in comparison with the typical brittle failures occurring in the interfacial IMCs.

The work on ductile-to-brittle transition (DBT) of Sn–0.7Cu solder has been investigated by Lambrinou et al. [102]. The test specimen was Charpy V-notch (CVN) rectangular bar of $5\times5\times55\ mm^3$ dimension having 1.3 mm deep notch. Impact tests were carried out on the specimens. The solder CVN specimen was tested in impact between −190 and 100 °C. The solder alloy undergoes ductile to brittle transition in its fracture behavior, because as the test temperature decreases the impact resistance of the solder decreases significantly. The maximum impact energy change (ΔE_{max}) during solder embrittlement was found to be around 4.42 J, where $\Delta E_{max} = \Delta E_{ductile}$ (maximum impact energy in ductile regime) $- \Delta E_{brittle}$ (minimum impact energy in brittle regime). No fracture was observed between room temperature and −125 °C (Fig. 45). At −135 °C, the solder behaved effectively as a brittle material. The fractured Sn–0.7Cu solder that failed in brittle behavior showed the co-existence of two types of fracture: a stepwise, cleavage-like (transgranular) fracture and an intergranular fracture (Figs. 46 and 47). The intergranular type of failure is associated with the separation of Sn–Cu_6Sn_5 eutectic grains from the Sn solder matrix. The cleavage-like type of fracture is associated with the fracture of Sn. Ductile-to-brittle transition in Sn–0.7Cu solder was completed within a narrow temperature range. The embrittlement of this solder was attributed to the embrittlement of the β-Sn matrix, since the volume fraction of IMCs that could contribute to the solder embrittlement process is very limited.

6. Reliability studies in ball grid array and flip chip electronic packaging

The solder joint reliability of ball-grid-array (BGA) is one of the major concerns to be considered in electronic applications. Elevated atmospheric temperatures on the solder joint result in the growth of intermetallic compounds (IMCs), which weaken the strength of solder joint because of their brittleness and weakness. Therefore, it is necessary to understand and control the factors that govern the kinetics of interfacial reactions especially for BGA and flip chip technologies.

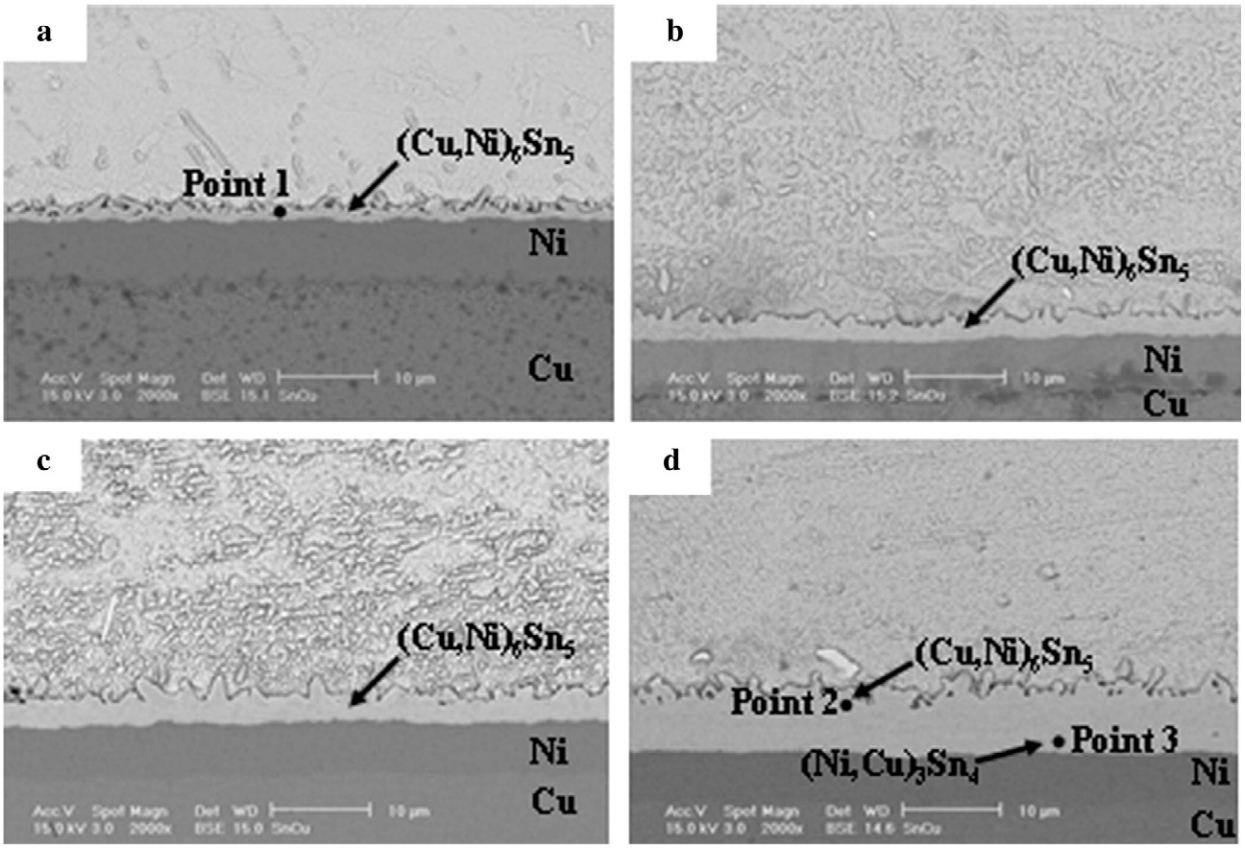

Fig. 48. SEM micrographs of the interfaces between the Sn–0.7Cu solder and Ni/Cu substrate: (a) as-reflowed, (b) after aging at 150 °C for 100 days (c) after aging at 170 °C for 30 days and (d) after aging at 170 °C for 50 days.
[103].

Yoon et al. [103] investigated the reliability and interfacial reaction of BGA Packages between the eutectic Sn–Cu solder alloy and the Au/Ni/Cu substrate by solid-state isothermal aging at temperatures between 70 °C and 170 °C for 0 to 100 days. A $(Cu,Ni)_6Sn_5$ layer was observed in samples aged at 70–150 °C. After 50 days of isothermal aging at 170 °C, the solder/Ni interface exhibited a duplex structure of $(Cu,Ni)_6Sn_5$ and $(Ni,Cu)_3Sn_4$ (Fig. 48). The shear strength extensively decreased after aging for 1 day and then remained the same for further prolonged aging. The shear strength of the solder sample aged at higher temperature was found to be surprisingly higher due to the varying solubility of Cu solubility in the Sn matrix at different aging temperatures. The fracture always occurred in the bulk solder (Fig. 49).

Microstructure evolution and shear strength of eutectic Sn–0.7Cu lead-free BGA solder balls were also investigated by Wu and Law [104]. Sn–0.7Cu solder balls were attached on Au/Ni/Cu BGA metallization pad to study the evolution of microstructure at the interface at 150 °C. As-reflowed Sn–0.7Cu solder ball exhibited Cu_6Sn_5 in the bulk and $AuSn_4$ segregated along the boundary of β-Sn grains. Au metallization layer was dissolved completely into the molten solder during as-reflow process. At the solder/pad interface, the Cu–Sn–Ni ternary intermetallic layer was observed and was found to be $(Cu,Ni)_6Sn_5$. On further aging, the $AuSn_4$ IMCs were coarsened. After thermal aging for 500 h the Cu–Sn–Au phase was observed in the bulk of solder alloy. The $(Cu,Ni)_6Sn_5$ layer at the interface was found to be thick due to aging (Fig. 50). Sn–0.7Cu exhibited good resistance to thermal aging with a ball shear strength maintained at about 1.5 to 1.6 kgf. Wu and Law suggested that Sn–0.7Cu solder is much stable and would act as solder ball material in BGA.

Frear et al. [105] carried out investigation to find the optimal lead free solder alloy which can be efficiently used for flip chip electronic packaging applications in terms of reliability of the joint and intermetallic formation concerns. Three lead free solder alloys (Sn–3.5Ag, Sn–0.7Cu, and Sn–3.8Ag–0.7Cu) were selected to examine the intermetallic reaction products at the interface and to carry out the shear strength and thermomechanical fatigue reliability tests. The reaction behavior and reliability of these solders were determined in a flip-chip design using a TiW/Cu, electrolytic nickel, and electroless Ni–P/Au under-bump metallization. It was found that Sn–0.7Cu solder exhibited a large grain structure and the Sn–3.5Ag and Sn–3.8Ag–0.7Cu have a fine lamellar two-phase structure of Sn and Ag_3Sn (Fig. 51). During reflow, growth rate of the intermetallic was faster for all solder alloys. The strength of Sn–0.7Cu is found to be lower but had the best thermomechanical fatigue behavior. Failures occurred near the interface for Sn–3.5Ag and Sn–3.8Ag–0.7Cu alloys, except Sn–0.7Cu, which failed in the center of the joint and deformed by sliding of grain. After carrying out the reliability tests, Frear et al. concluded that, eutectic Sn–0.7Cu is the optimal solder alloy for flip-chip applications. Data on mechanical properties of eutectic Sn–0.7Cu solder under various conditions reported in the literature are given in Table 15. Table 16 gives data on creep stress exponents, activation energy, resistivity and surface tension of Sn–0.7Cu solder samples (bulk and joint).

7. Summary

Sn–0.7Cu is least expensive among all other lead free solders and costs only 30% higher than the eutectic Sn–Pb solder. It is

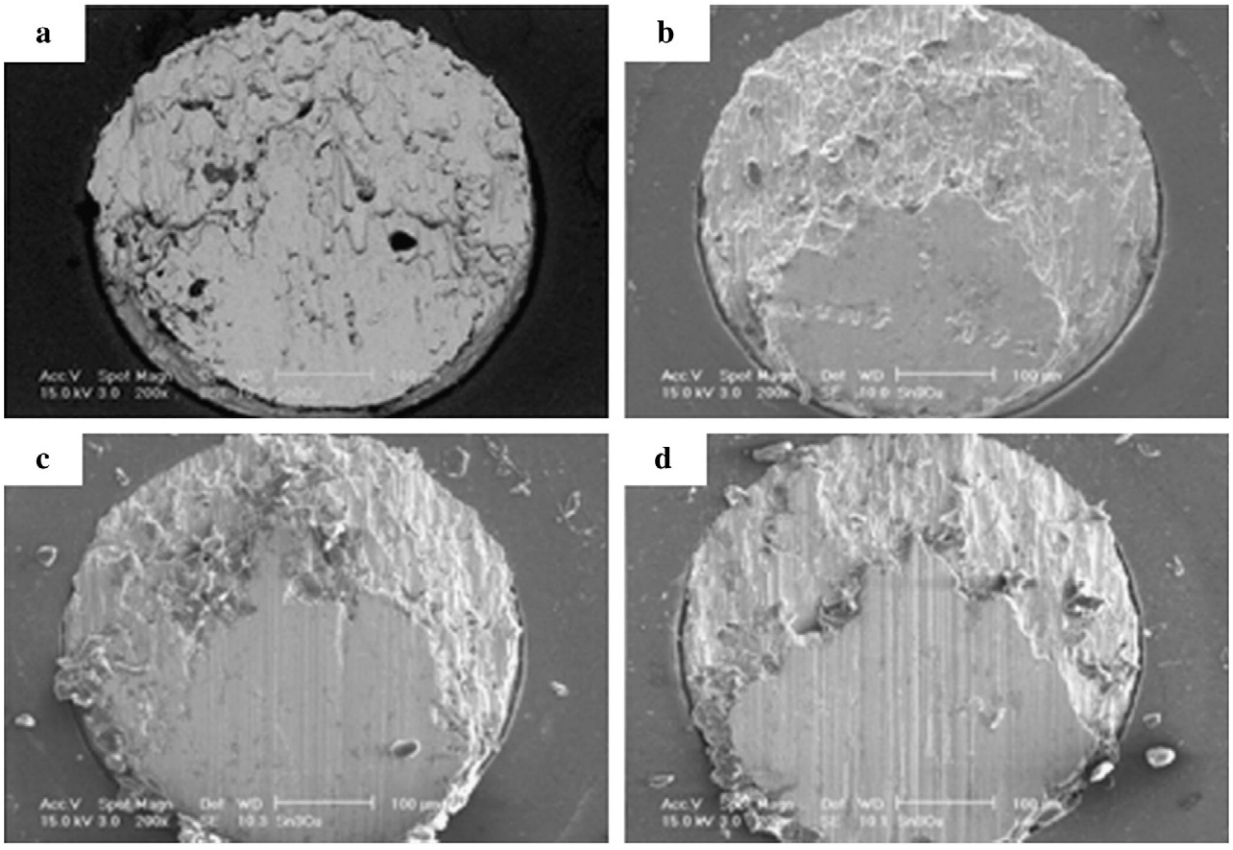

Fig. 49. SEM micrographs of the fracture surfaces: (a) as-reflowed, (b) 150 °C, 1 day (c) 100 °C, 50 days and (d) 150 °C, 50 days. [103].

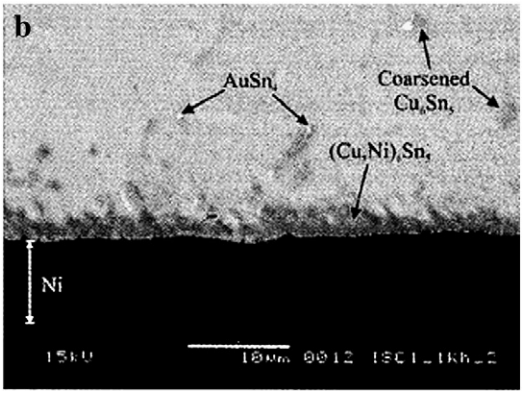

Fig. 50. BSE micrograph of as-reflowed Sn–0.7Cu at the interface aged for 1000 h. [104].

mainly used for wave soldering applications in electronics and automobile industry. The temperature and type of flux has a significant effect on wettability of Sn–0.7Cu solder on various substrates. In most of the cases, with increase in temperature, the wetting force increases and contact angle decreases. For the solder alloy, R flux is found to be not suitable on Cu and Ni substrates. The alloy shows a smaller equilibrium contact angle on the IMC (Cu_6Sn_5/Cu_3Sn) surface than the virgin copper substrate. The suitable temperature to perform soldering of eutectic Sn–0.7Cu alloy is 303 °C (603 K). The solder exhibits a smallest value of surface tension at this temperature.

It is found that, the surface roughness of Cu substrate had no significant influence on the spreading behavior of eutectic Sn–Cu lead free solder. The formation of tin pest of Sn–0.7Cu alloy is delayed in rolled high purity Sn–0.7Cu ingots stored at sub zero temperature for long period of time. The rolling process will elongate the Sn particles, increase the areas of grain boundaries, make the Cu_6Sn_5 IMC into smaller and generate the dislocations and residual stresses. These factors will strengthen the alloy, making the allotropic change of β-Sn to α-Sn more difficult. However, the impurities present in the solder alloy may promote the formation of Sn pest.

On copper substrates, solder alloy exhibits a layer of Cu_3Sn at the interface and Cu_6Sn_5 layer on top of Cu_3Sn. As the reflow and aging temperature increases the thickness of intermetallic layer also increases. Solder on silver substrate showed a continuous thin IMC layer devoid of protrusions, with Ag_3Sn IMC within the solder field. For eutectic Sn–Cu/Ni, two kinds of detachments will exist. During initial reaction, the Cu_6Sn_5 layer fractures and loose layer separate from the attached Cu_6Sn_5 layer. At the final stage, the Cu_6Sn_5 layer separates from Ni_3Sn_4 phase adjacent to the nickel based metal. The electromigration induced failure and degradation of joint strength are common in Cu based bond pads. This could be prevented by using Co as a metal bond.

For the solder/Ni-20 at.% Co substrate combination, the $(Ni_x,Cu_y,Co_{1-x-y})Sn_2$ intermetallic compound layer formed early, after about 60 s of reflow. After extensive reflow, needle-like interfacial $(Ni_x,Co_y,Cu_{1-x-y})_3Sn_4$ phase formed above the continuous $(Ni_x,Cu_y,Co_{1-x-y})Sn_2$ compound layer. The growth rate of $PtSn_4$ on solder/platinum substrate is found to be very slow and obeys parabolic law. This is one of the advantages of using platinum as metallization layer.

The mechanical behavior of interfacial intermetallic compounds (IMCs) plays a key role while determining the reliability of solder joints. Nanoindentation and microhardness methods are useful in assessing the behavior of the interfacial IMC. The thickness of IMC is found to be important. There exists a critical value of thickness beyond which the failure occurs within the IMC instead of in bulk of the solder.

The unified constitutive equation has been used for solders since 1982. The advantage is that it combines the plastic deformation and creep into one component. However it cannot account for the local microstructure. With the continuous miniaturization of solder interconnections, one solder joint can contain one or a few grains and hence the constitutive equation based on polycrystalline bulk solder might not be accurate enough. Future work should therefore be directed towards developing microstructure dependent models for predicting interface damage in solder joints involving Sn–0.7Cu solder.

Wettability and the formation of interfacial IMCs at the interface are very much interrelated and cannot be separately studied. Both have a significant effect on the quality of the solder joint. For a better understanding of the wetting behavior, the formation of interfacial IMCs at the interface and mechanical behavior of eutectic Sn–0.7Cu alloy, the future work should also focus on evolving a standard procedure involving sequential assessment of wetting behavior, evolution of interfacial IMCs between solder and the substrate followed by measurement of mechanical properties of the solder joint formed. The addition of nanoparticles or elements like Ni and Zn to the solder alloy offers further scope for the development of eutectic Sn–Cu alloy as a universal lead free solder material.

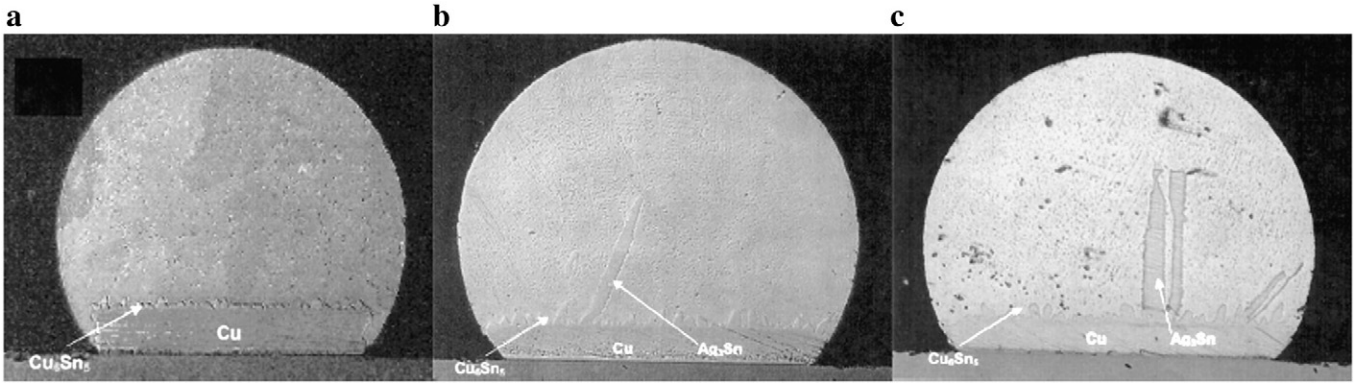

Fig. 51. Microstructure of (a) Sn–0.7Cu, (b) Sn–3.5Ag, and (c) Sn–3.8Ag–0.3Cu solder in a flip-chip bump on a copper UBM. [105].

Table 15
Data on mechanical properties of solder samples (bulk and joint).

Solder/substrate	Process/specimen preparation	Reflow (s)	Testing method	Strain rate γ (s^{-1})	UST (MPa)	Young's modulus E (Gpa)	Fracture toughness MPa $m^{1/2}$	YS (MPa)	UTS (MPa)	Vickers microhardness (HV)	I.M. (E) GPa	Hardness (H)	Reference
Sn–0.7Cu/Cu										16			[82]
Sn–0.7Cu	QC		Shear	10^{-5}	14. ± 0.01								[83]
Sn–0.7Cu	FC		Shear	10^{-5}	11.5 ± 0.016								[83]
Sn–0.7Cu	QC		Shear	10^{-4}	15.5 ± 0.01								[83]
Sn–0.7Cu	FC		Shear	10^{-4}	15.6 ± 0.01								[83]
Sn–0.7Cu	QC		Shear	10^{-3}	24.4 ± 0.011								[83]
Sn–0.7Cu	FC		Shear	10^{-3}	16.6 ± 0.01								[83]
Sn–0.7Cu	QC		Shear	10^{-2}	24.1 ± 0.006								[83]
Sn–0.7Cu	FC		Shear	10^{-2}	24.2 ± 0.011								[83]
Sn–0.7Cu	QC		Shear	10^{-1}	32.8 ± 0.005								[83]
Sn–0.7Cu	FC		Shear	10^{-1}	31.6 ± 0.01								[83]
Sn–0.7Cu						26							[83]
Sn–0.7Cu	WQ[a]							15.3	19.44				[84]
Sn–0.7Cu	AC							16	21.58				[84]
Sn–0.7Cu	As-soldered		Nanoindentation	1.8×10^{-3}							41 ± 3	0.3 ± 0.01	[87]
Sn–0.7Cu	As-soldered		Nanoindentation	1.8×10^{-2}							52 ± 1	0.51 ± 0.03	[87]
Sn–0.7Cu	As-soldered		Nanoindentation	1.8×10^{-1}							63 ± 4	0.72 ± 0.05	[87]
Sn–0.7Cu/Ni–Pd		45					9.13						[92]
Sn–0.7Cu/Ni–Pd		180					8.19						[92]
Sn–0.7Cu/Cu		45					9.13						[92]
Sn–0.7Cu/Cu		90					9.23						[92]
Sn–0.7Cu/Cu		180					7.55						[92]
Sn–0.7Cu			X-ray diffraction			64.1							[93]
Sn–0.7Cu			Ring and plug		27 ± 1.0[b]								[107]
Sn–0.7Cu			Ring and plug		13.3 ± 0.4[c]								[107]
Sn–0.7Cu			Flip-chip		9.2								[106]
Sn–0.7Cu			As-quenched melt-spun					61.31 ± 0.17		196.21 ± 0.54			[94]
Sn–0.7Cu	Aged at 150 °C for 20 h		Tensile						30				[98]
Sn–0.7Cu	Nanocomposite (sintered)		Tensile					17 ± 1	20 ± 1	8.8 ± 0.2			[109]

I.M.: indentation modulus.
Ultimate shear strength (UST), YS (yield strength), UTS (ultimate tensile strength).
[a] Average value of 3 trials (Fig. 34a).
[b] For displacement rate at 0.1 mm/min at room temperature.
[c] For displacement rate at 0.1 mm/min at 125 °C.

Table 16
Data on creep stress exponents, activation energy, resistivity and surface tension of Sn–0.7Cu solder samples (bulk and joint).

Solder	Preparation technique	Temperature range (°C)	Creep stress exponent (n)	Activation energy (kJ/mol)	Resistivity $\times 10^{-8}$ (ohm.m)	Reference
Sn–0.7Cu	Single roller melt-spinning technique				11.14	[99]
Sn–0.7Cu	As-quenched meltspun				11.14 ± 0.2	[94]
Sn–0.7Cu		25 °C to 120 °C	7[a]	56.5 ± 0.5		[99]
Sn–0.7Cu		25 °C	10[a]			[99]
Sn–0.7Cu		95 °C	8[b]			[99]
Sn–0.7Cu		120 °C	7[b]			[99]
Sn–0.7Cu/Cu		25 °C to 60 °C LSR	4			[99]
Sn–0.7Cu/Cu		95 °C to 120 °C LSR	4			[99]
Sn–0.7Cu/Cu		25 °C to 60 °C HSR	4			[99]
Sn–0.7Cu/Cu		95 °C to 120 °C HSR	4			[99]
Sn–0.7Cu/Cu		25 °C to 60 °C LSR	4			[99]
Solder/Cu/Ni–Au		LSR	3.5	90		[110]
		HSR	8.9	85		[110]

Surface tension of Sn–0.7Cu: 491 mN/m in air and 461 mN/m in nitrogen atmosphere [108].
LSR: low stress regime, HSR: high stress regime.
[a] For cooling rate 0.1 °C/s (furnace cooling).
[b] For cooling rate 24 °C/s (water cooling).

References

[1] Manko HH, Solders and Soldering, 2nd edition, McGraw-Hill Publications, New York. 1964; p.1-20, 55–154 & 109–110.
[2] Hwang JS. Implementing lead-free electronics. McGraw-Hill; 2005. p. 10–90.
[3] Seo SK, Kang SK, Shih DY, Lee HM. J Electron Mater 2009;38(2):257–65.
[4] Kumar G, Prabhu KN. Proc. International conference on advanced materials and composites (ICAMC) Trivandram, India; Oct 24–26, 2007. p. 535–40.
[5] Mayappan R, Ismail AB, Ahmed ZA, Ariga T, Hussain LB. Jurnal Teknologi 2007;46 (C):1–14.
[6] Chen YY, Duh JG. J Mater Sci: Mater Electron 2000;11:279–83.
[7] Hu Q, Lee ZS, Zhao ZL, Lee DL. International conference on Asian green electronics; 2005. p. 156–60.
[8] Satyanarayan, Prabhu KN. J ASTM Int 2010;7(9):JAI103052.
[9] Islam RA, Chan YC, Jillek W, Islam S. Microelectron J 2006;37:705–13.
[10] Bastow E. Solder families and how they work. Adv Mater Process 2003;3:26–9.
[11] Shen J, Liu Y, Houxiu Gao YH. J MaterSci: Mater Electron 2007;8:1235–8.
[12] Liu M, Xian AP. J Electron mater 2009;38(11):2353–61.
[13] Kang SK. Metals Mater 1999;5(6):545–9.
[14] Alam ME, Nai SML, Gupta M. J Electron mater 2009;38(12):2479–88.
[15] Chukka RN, Telu S, Bhargava NRMR, Chen L. J Mater Sci: Mater Electron 2010;22 (3):281–5.
[16] Lee NC. International symposium on microelectronics, Boston MA, vol.4339; September 20–22, 2000. p. 541–50.
[17] Grusd A. Lead free solders in electronics. http://www.xs4all.nl/~tersted/PDF_files/Heraeus/SMI98NoPb.pdf accessed on 10-12-2010.
[18] Lee NC. Adv Microelectron 1999:29–36.
[19] Oh TS, Ha JS, Tu KN. http://www.electrochem.org/dl/ma/202/pdfs/0551.PDF accessed on 26-12-10.
[20] Chellaih T, Kumar G, Prabhu KN. Mater Des 2007;28:1006–11.
[21] Braunovic M, Konchits V, Myshkin N. Electronic connections. Boca Raton, London, New York: CRC press, Taylor & Francis Group, LLC; 2006. p. 309–67.
[22] Frear D, Grivas D, Morris JW. J Electron Mater 1987;16(3):181–6.
[23] Nalagatla DR, Master of Science thesis, The Graduate School, University of Kentucky 2007.
[24] Abtew M, Selvaduary G. Mater Sci Eng R 2000;27:95–141.
[25] Sweatman K, Nishimura T. IPC printed circuits expo®, APEX® and the designers summit; 2006.
[26] Sweatman K, Nishimura T. Proceedings of the ECWS 10 conference, Anaheim, USA; February 22–24, 2005.
[27] Smith III EB. International conference on lead-free electronic components and assemblies, San Jose California; May 2002. p. 3.
[28] Zarrow P. The real cost of lead free soldering. http://www.itmconsulting.org/Column34-Real%20Cost%20of%20Lead-Free%20Soldering.pdf 2011 (accessed on 10-1-2011).
[29] Report on the workshop on modeling and data needs for lead-free solders sponsored by NEMI, NIST, NSF, and TMS. http://www.nemi.org/PbfreePUBLIC/index.html 2001 (accessed on 10-1-2011).
[30] Prabhu KN, Kumar G. J Electron Packag 2010;132:041001.
[31] Kumar G, Prabhu KN. J ASTM Int 2010;7(5):JAI103055.
[32] Kumar G, Prabhu KN. Adv Colloid Interface Sci 2007;133:61–89.
[33] Takao H, Tsukada T, Yamada K, Yamashita M, Hasegawa H. R&D review of Toyota CRDL, 39; 2004. p. 2.
[34] Matsumoto T, Nogi K. Ann Rev Mater Res 2008;38:251–73.
[35] Novak T, Steiner F. Electronic technology. 32nd International spring seminar ISSE; 2009.
[36] Rizvi MJ, Bailey C, Chan YC, Lu H. Electronics system integration technology conference Dresden, Germany; 2006. p. 145–51.
[37] Hwang JS. Int J Microcircuits Electron Packag (IMPS) 2001;24(4):316–27.
[38] Mario FA, Acoff VL. J Electron Mater 2004;33(12):1452–8.
[39] Mario FA, He M, Acoff VL. J Electron Mater 2006;35(7):1530–6.
[40] Wang H, Zhao H, Sekulic DP, Qian Y. J Electron Mater 2008;37(10):1640–6.
[41] Zhao N, Pan XM, Yu DQ, Ma HT, Wang L. J Electron Mater 2009;38(6):828–33.
[42] Zhao H, Nalagatla DR, Sekulic DP. J Electron Mater 2009;38(2):284–91.
[43] Humpston G, Jacobson MD. Principles of soldering, ASM International; 2004. p. 20–2.
[44] Shapiro EA. Welding Journal 2007:33–4.
[45] Zhao H, Wang HQ, Sekulic DP, Qian YY. J Electron Mater 2009;38(9):1846–54.
[46] Sattiraju SV, Johnson RW, Genc DZ, Bozack MJ. IEEEICPMT Int'l electronics manufacturing technology symposium; 2000. p. 253–62.
[47] Hsu HJ, Hang JT, Chao PS, Shih SH. Microelectron Engg 2008;85:1595–601.
[48] Li X, Zhang F, Zu F, Lv X, Zhao Z, Yang D. J Alloys Compd 2010;505:472–5.
[49] Jung I, Cho MG, Lee HM. J Mater Sci: Mater Electron 2009;38(11):2301–7.
[50] Wang H, Wang F, Ma X, Liu J, Qian Y. IEEE 6th international conference on electronic packaging technology; 2005.
[51] Wang H, Wang F, Gao F, Ma X, Qian Y. J Alloys Compd 2007;433:302–5.
[52] Chang HY, Chen SW, Wong DSH, Hsu HF. J Mater Res 2003;18:1420–8.
[53] Rizvi MJ, Bailey C, Chan YC, Lu H. J Alloys Compd 2007;438:116–21.
[54] Seo SK, Kang SK, Shih DY, Lee HM. Microelectron Reliab 2009;49:288–95.
[55] Lauro P, Kang SK, Choi WK, Yuan Shih D. J Electron Mater 2003;32(12):1432–9.
[56] Nogita K, Read J, Nishimura T, Sweatman K, Suenaga S, Dahle AK. Mater Trans Jpn Inst Met 2005;46(11):2419–25.
[57] Mathiesen RH, Arnberg L, Mo F, Weitkamp T, Snigirev. Phys Rev Lett 1999;83 (24):5062–5.
[58] Shen J, Liu YC, Gao HX. J Mater Sci 2007;42:5375–80.
[59] Peng W. Microelectron Reliab 2009;49:86–91.
[60] Kariya Y, Williams N, Gagg C, Plumbridge WJ. JOM 2001;53(6):39–41.
[61] Joo YJ, Takemoto T. Mater Lett 2002;56(5):793–6.
[62] Prabhu KN, Satyanarayan, Mater Sci Technol in press, http://www.ingentaconnect.com/content/maney/mst/pre-prints/026708310X12815992418337.
[63] Bayes M. Materials matter: solder joint reliability, PCB design 007. http://www.pcbdesign007.com/pages/zone.cgi?a=21806 2008 accessed on April-2010.
[64] Laurila T, Vesa V. Intermetallic compound layers related to lead-free soldering. http://www.scitopics.com/Intermetallic_compound_layers_related_to_lead_free_soldering.html 2010 SciTopics, accessed on July 13, 2010.
[65] Madeni J, Liu S, Siewert T. 2nd International brazing and soldering conference (ISBC); 2003.
[66] Nogita K, Gourlay CM, Nishimura T. JOM 2009;61(6):45–51.
[67] Dariavach N, Callahan P, Liang J, Fournelle R. J Electron Mater 2006;35(7): 1581–91.
[68] Zhao N, Pan X, Ma X, Dong C, Guo S, Lu W, et al. 13th International conference on liquid and amorphous metals. J Phys: Conf Ser 2008;98:012029.
[69] Suha JO, Tu KN, Tamura NJ. Appl Phys 2007;102:063511.
[70] Suha JO, Tu KN, Lutsenko GV, Gusak AM. Acta Mat 2008;56:1075–83.
[71] Lu CC, Wang SJ, Liu CY. J Electron Mater 2003;32(12):1515–22.
[72] Vianco PT, Martin JJ, Wright RD, Hlava PF. Metall Mater Trans 2006;37A:1551–61.

[73] Chen SW, Wang CH, Lin SK, Chiu CN, Chen CC. JOM 2007:39–43.
[74] Yoon JW, Kim SW, Jung SB. J Alloy Compd 2005;5:82–9.
[75] Yoon JW, Jung SB. Microelectron Reliab 2006;46:905–14.
[76] Huang ML, Loeher T, Manessis D, Boettcher L, Ostmann A, Reichl HJ. Electron Mater 2006;35(1):181–8.
[77] Cho MG, Kang SK, Seo SK, Shih DY, Lee HM. J Electron Mater 2009;38(11): 2242–50.
[78] Huang KC, Shieu FS, Huang TS, Lu CT, Chen CW, Tseng HW, et al. J Electron Mater 2010;39(11):2403–11.
[79] Meagher B, Schwarcz D, Ohring M. J Mater Sci 1996;31:5479–86.
[80] Yang SC, Chang WC, Wang YW, Kao CR. J Electron Mater 2009;38:1.
[81] Kim TH, Kim YH. JOM 2004:45–9.
[82] Bae KS, Kim SJ. J Mater Res 2002;17(4):743–6.
[83] Maveety JG, Liu P, Vijayen J, Hua F, Sanchez EA. J Electron Mater 2004;33(11): 1355–62.
[84] Madeni J, Liu S, Siewert T. Proc. ASM 2002. http://www.boulder.nist.gov/div853/Publication%20files/NIST_ASM_Pb_free_casting.pdf July 13, 2010 on.
[85] Chromik RR, Vinci RP, Allen SL, Notis MR. JOM 2003:66–9.
[86] Oliver WC, Pharr GM. J Mater Res 1992;7:1564.
[87] Rosenthala Y, Sterna A, Cohenb SR, Eliezer D. Mater Sci Eng 2010;A527:4014–20.
[88] Bai N, Chen X. Int J Plasticity 2009;25:2181–203.
[89] Roe KL, Siegmund T. Eng Fract Mech 2003;70:209–32.
[90] Erinc M, Schreurs PJG, Geers MGD. Cohesive zones for fatigue damage in solder joints. http://74.125.155.132/scholar?q=cache:pBlWaTLc6TsJ:scholar.google.com/&hl=en&as_sdt=0,5 accessed on 25-04-2011.
[91] Abdul-Baqi A, Schreurs PJG, Geers MGD. Int J Solids Struct 2005;42:927–42.
[92] Hayes SM, Chawla N, Frear DR. Microelectron Reliab 2009;49:269–87.
[93] El-Ashram TJ. Mater Sci: Mater Electron 2005;16:501–5.
[94] El-Ashram T, Shalaby RM. J Electron Mater 2005;34(2):212–5.
[95] Bai N, Chen X, Fang ZJ. Electron Mater 2008;37(7):1012–9.
[96] Song HG, Morris Jr JW, Hua F. Lawrence Berkeley National Laboratory. LBNL paper LBNL-50005; 10-12-2010 http://escholarship.org/uc/item/2dn704z0. accessed on 10-12-2010.
[97] Huang ML, Wu CML, Wang L. J Electron Mater 2005;34(11):1373–7.
[98] Wu CML, Yu DQ, Law CMT, Wang L. J Electron Mater 2002;31:9.
[99] Sidhu RS, Deng X, Chawla N. Metall Mater Trans A 2008;39A:349–62.
[100] Shen YL, Abell KCR, Garrett SE. Int J Damage Mech 2004;13:225–39.
[101] Telang AU, Bieler TR. JOM 2005:44–9.
[102] Lambrinou K, Engelmaier W. J ASTM Int 2010;7(7):JAI 103064.
[103] Yoon JW, Kim SW, Koo JM, Kim DG, Jung SB. J Electron Mater 2004;33(10): 1190–9.
[104] Wu CML, Law CMT. HDP '04. proc. 6th IEEE CPMT conference; 2004. p. 47–51.
[105] Frear DR, Jang JW, Lin JK, Zhang C. JOM 2001:28–33.
[106] Kang SK, Lauro P, Shih DY, Henderson DW, Puttlitz KJ. IBM J Res Dev 2005;49 (4/5):607–20.
[107] Foley JC, Gickler A, Leprevost FH, Brown D. J Electron Mater 2000;29(10): 1258–62.
[108] Glazer JJ. Electron Mater 1994;23(8):693–700.
[109] Nai SML, Kuma JVM, Alam ME, Zhong XL, Babaghorbani P, Gupta M. J Mater Eng Perform 2010;19(3):335–41.
[110] Song HG, Morris Jr JW, Hua F. JOM 2002:30–2.